5-2009

Electron Density and Electron Neutral Collision Frequency in the Ionosphere Using Plasma Impedance Probe Measurements on Sounding Rockets

Swadesh Patra
Utah State University

ELECTRON DENSITY AND ELECTRON NEUTRAL COLLISION FREQUENCY IN THE IONOSPHERE USING PLASMA IMPEDANCE PROBE MEASUREMENTS ON SOUNDING ROCKETS

by

Swadesh Patra

A thesis submitted in partial fulfillment
of the requirements for the degree

of

MASTER OF SCIENCE

in

Electrical Engineering

Approved:

Dr. Edmund Spencer Major Professor	Dr. Charles M. Swenson Committee Member
Dr. Reyhan Bakhtur Committee Member	Dr. Byron R. Burnham Dean of Graduate Studies

UTAH STATE UNIVERSITY
Logan, Utah

2009

Abstract

Electron Density and Electron Neutral Collision Frequency in the Ionosphere Using Plasma Impedance Probe Measurements on Sounding Rockets

by

Swadesh Patra, Master of Science

Utah State University, 2009

Major Professor: Dr. Edmund Spencer
Department: Electrical and Computer Engineering

The Plasma Impedance Probe (PIP) is an RF-instrument that is used to measure plasma electron density and electron neutral collision frequency. Radio Frequency probe techniques for the determination of plasma parameters are attractive especially because the RF response is not susceptible to spacecraft charging problems at frequencies above the electron plasma frequency where ion sheath effects are negligible. The work done in this thesis is presented as a compendium of two papers, the first paper dealing with PIP measurements on a sounding rocket mission and the second being a qualitative study of the effects of spacecraft aerodynamics on the impedance of antennas.

Swept Impedance Probe measurements in a sporadic E-Layer observed during the Sudden Atomic Layer (SAL) sounding rocket mission are analyzed in the first paper to obtain absolute electron densities and electron neutral collision frequencies accurately. Three sets each of upleg and downleg impedance data are selected for the analysis. Initial estimates of the plasma parameters are obtained through a least mean square fit of the measured impedance data against the analytical impedance formula of Balmain. These initial parameters are used as a starting point to drive a finite difference computational model of an antenna immersed in a plasma called the Plasma Fluid Finite Difference Time Domain

(PF-FDTD) model. The parameters are then tuned until a close fit is obtained between the measured impedance data and the numerical impedance data calculated by the PF-FDTD simulation. The electron neutral collision frequencies obtained from the more accurate PF-FDTD simulation were up to 20% lower than the values predicted by Balmain's formula. The obtained collision frequencies are also lower than the quiet time values predicted by Schunk and Nagy when used in conjunction with neutral densities and electron temperature from the MSISE-90 model.

Plasma impedance probe measurements on sounding rockets are affected by aerodynamics of the spacecraft body. The second paper analyzes the effects of density gradients and wake effects on the impedance of a dipole antenna. A Direct Simulation Monte Carlo (DSMC) code is used to simulate the aerodynamic conditions encountered during a typical sounding rocket flight. Conical electron density flow structure is used to approximate the density distribution around a spinning rocket flying through the lower ionosphere. The PF-FDTD code is modified to simulate the impedance of a dipole antenna under different flow conditions. A methodology is developed to find correction factors to rectify errors introduced due to spin modulation on sounding rockets, and the technique is applied for the SAL sounding rocket mission.

(69 pages)

Contents

List of Tables

List of Figures

Chapter 1

Introduction

Any material is characterized by parameters that define the state and properties of the matter. For ordinary materials the most general set of parameters are the density, pressure, and temperature. Plasma is defined as a quasi-neutral collection of charged particles which exhibit collective behavior. Considerably more number of parameters are needed to satisfactorily characterize a plasma. Certain fundamental plasma parameters that are relevant to the work done in this thesis are the electron-plasma frequency (ω_{pe}) which is proportional to the ambient electron density, electron cyclotron frequency (Ω_{ce}) that is proportional to the external magnetic field, and the electron-neutral collision frequency (ν_{en}). For most ionospheric conditions the electron fundamental frequencies would be higher than the corresponding ion frequencies, hence the plasma frequency (ω_p) has been used interchangeably with the electron-plasma frequency (ω_{pe}).

Multiple methods and instruments have been developed over the years to measure these parameters. One of the popular instruments that is used to measure electron density in plasma environments is the plasma impedance probe (PIP). Impedance probes have been used to measure electron densities in the ionosphere as well as in laboratory conditions. Although the underlying principle is simple, the plasma environments and the deployment of the instrument present every measurement with its own set of issues. Lower and extremely high density regions in the ionosphere challenge the operating ranges of the instrument electronics. The assumption used in the analytical theories used to analyze the impedance data do not always hold true in the medium under observation. Even the fact that these instruments are deployed on a moving spacecraft complicate the analysis. In this thesis we have tried to quantify and qualitatively analyze some of these problems encountered by plasma impedance probes.

Thesis Outline

The input impedance of an electrically short antenna can be used to measure plasma densities, electron neutral collision frequency, and potentially the electron temperature. This thesis is based on the work done in interpreting impedance data to deduce ionospheric plasma parameters using Plasma Fluid Finite Difference Time Domain (PF-FDTD) numerical simulation which have led to two papers.

In Chapter 2 the working principle of the impedance probe is discussed. The analytical theories traditionally used to analyze impedance data are also briefly explained. The PF-FDTD simulation developed by Ward [1] is also explained in this chapter.

Chapter 3 represents the work done to extract electron density and electron-neutral collision frequency from the PIP on SAL sounding rocket using PF-FDTD and has been published in Journal of Geophysical Research [2]. Chapter 4 is a short chapter which explains the frequency scaling property observed in the linearized PF-FDTD simulations and the algorithm that is used to automate the matching procedure of Chapter 3 using this property.

Effect of spacecraft aerodynamics on impedance probe measurement is explored in Chapter 5, the results of which will soon be submitted to a relevant journal. Finally, Chapter 6 summarizes the work done in this thesis and discusses avenues for future work.

Chapter 2

Plasma Impedance Probe

Any antenna that is used to actively probe the plasma medium to extract information about its dielectric properties from its input impedance may be called as an plasma impedance probe. A linear wire antenna is considered as an infinitesimal dipole if its dimensions are small compared to the operating wavelength (i.e., length $l << \lambda$ and radius $a << \lambda$). The complex power moving in the radial direction for a lossless infinitesimal dipole is given by [3]:

$$P = \eta \frac{\pi}{3} \left| \frac{I_o l}{\lambda} \right|^2 \left[1 - j \frac{1}{(kr)^3} \right], \tag{2.1}$$

where $\eta =$ the intrinsic impedance, and $I_o =$ the constant current distribution.

It is clearly evident from (2.1) that the reactive power density dominates for small values of kr. A constant current is assumed for this case, which is not physically realizable for most cases. A better approximation of the current distribution for short dipoles ($\lambda/50 < l \leq \lambda/10$) is a triangular variation across the length of the dipole. The real part of the input impedance of a lossless antenna is the antenna's radiation resistance. The radiation resistance of a short dipole assuming triangular current distribution is given by:

$$R_r = \frac{2P_{rad}}{|I_o|^2} = 20\pi^2 (\frac{l}{\lambda}). \tag{2.2}$$

From the above equation and (2.1) for a short dipole we can infer that for an electrically short antenna ($l << \lambda$) the radiation resistance is negligible for longer wavelengths and the impedance of a short dipole is predominantly capacitive.

Assuming the impedance of a dipole to be completely capacitive, the fundamental impedance of the antenna in freespace can be written as:

$$Z_{antenna} = \frac{-j}{\omega C_o}, \tag{2.3}$$

where C_o = Freespace Capacitance of dipole antenna, $\omega = 2\pi f$ is the radian drive frequency, and f is the frequency in Hz.

2.1 Principle of Operation: Impedance Probe

The impedance of a short dipole antenna immersed in a plasma departs from its free space value due to the properties of the surrounding medium. The dielectric properties of the plasma are a function of the propagation frequency, ambient plasma density, magnetic field, collision frequency, and angle between the propagation direction and the magnetic field.

When an antenna emits radio frequency waves, the fields from these waves excite the nearby electrons which affect the antenna impedance in the medium. For an electrically short antenna radiating waves at frequencies much greater than the electron plasma and gyrofrequencies, its impedance is a capacitive reactance $1/\omega C$, where C is the antenna capacitance in the plasma. For $\omega >> \Omega_e$ and collisionless plasma ($\omega >> \nu_{en}$), the antenna departs from its free space capacitance, C_o, via [4]:

$$C = \epsilon_r C_o = \left(1 - \frac{\omega_p^2}{\omega^2}\right) C_o. \tag{2.4}$$

If the plasma is modeled as a lossey dielectric, due to electron neutral collisions (ν_{en}), the relative permittivity becomes:

$$\epsilon_r = 1 - \frac{\omega_p^2}{\omega^2 - j\omega\nu_{en}}. \tag{2.5}$$

The addition of a collision frequency converts the relative permittivity to a complex number, that when combined with the impedance calculation of a capacitor not only modifies the reactive component (X) of the impedance, but also adds a resistive component (R)

$$Z = \frac{1}{j\omega\epsilon_r C_o} = R + jX. \tag{2.6}$$

This resistive component captures the effect of energy lost as the electrons collide with the neutral particles. Solving (2.5) and (2.6) for the plasma frequency and electron neutral collision frequency in terms of the changes ΔX of the antenna reactance and resistance ΔR from their free space values gives the formulas referred to as Pfister's theory [1, 5, 6]:

$$\omega_p^2 = \omega^2 \left[\frac{\Delta X + \frac{\Delta R^2}{\Delta X}}{\Delta X + \frac{\Delta R^2}{\Delta X} + \frac{1}{\omega C_o}} \right], \tag{2.7}$$

$$\nu = \frac{\omega \frac{\Delta R}{\Delta X}}{1 + \omega C_o \left(\Delta X + \frac{\Delta R^2}{\Delta X} \right)}. \tag{2.8}$$

When ν is much smaller than ω, ΔR becomes negligible, simplifying equation 2.6 to:

$$\omega_p^2 = \omega^2 \left[\frac{\Delta X}{\Delta X + \frac{1}{\omega C_o}} \right]. \tag{2.9}$$

This limits the application of this theory to highly collisional plasma or cases where only electron density is required.

2.2 Balmain's Analytical Theory of Antenna Impedance

A number of analytical theories to predict the impedance of an electrically short dipole antenna in plasma environment have been proposed [7–10]. K. G. Balmain [10, 11] was the first to develop a relatively simple expression for thin dipole antenna immersed in a cold plasma with an arbitrarily oriented magnetic field using quasi-static electromagnetic theory for a line current distribution.

Using the dielectric tensor representation of relative permittivity for a cold, collisional, magnetized plasma typically is written as

$$\bar{\bar{\epsilon}}_r = \begin{pmatrix} \epsilon_1 & -\mathrm{j}\epsilon_2 & 0 \\ \mathrm{j}\epsilon_2 & \epsilon_1 & 0 \\ 0 & 0 & \epsilon_3 \end{pmatrix}, \tag{2.10}$$

$$\epsilon_1 = 1 - \frac{\omega_p^2(1 - \mathrm{j}\frac{\nu}{\omega})}{\omega^2(1 - \mathrm{j}\frac{\nu}{\omega})^2 - \Omega^2} \ , \tag{2.11}$$

$$\epsilon_2 = \frac{\omega_p^2\Omega/\omega}{\omega^2(1 - \mathrm{j}\frac{\nu}{\omega})^2 - \Omega^2} \ , \tag{2.12}$$

$$\epsilon_3 = 1 - \frac{\omega_p^2}{\omega^2(1 - \mathrm{j}\frac{\nu}{\omega})^2} \ , \tag{2.13}$$

Balmain converted the traditional free space impedance equation for a short dipole,

$$Z_{in} = \frac{1}{\mathrm{j}\omega\pi\epsilon_0 L'}\left(\ln\frac{L'}{R'} - 1\right) \ , \tag{2.14}$$

into that of a short dipole in a plasma by only replacing the effective half length (L) and radius (R)

$$L' = L\sqrt{\epsilon_1 T} \ , \tag{2.15}$$

$$R' = \frac{R}{2}\left(\frac{\epsilon_1\sqrt{\epsilon_3}}{\sqrt{T}} + \sqrt{\epsilon_1\epsilon_3}\right) \ , \tag{2.16}$$

$$T = \epsilon_0 sin^2\theta + \epsilon_1\cos^2\theta \ , \tag{2.17}$$

that are dependent upon the tensor dielectric representation ($\bar{\bar{\epsilon}}_r$ from 2.10) and the incident angle of the DC magnetic field (θ). Figure 2.1 shows the geometry of a dipole with feed current and magnetic field. The ion sheath is approximately taken into account by representing it as a sharply bounded vacuum gap of a finite thickness.

This yields vast improvements over the capacitive model of Pfister, specifically in the regions between the various critical plasma frequencies, where the simple scalar dielectric representation is no longer accurate. In fig. 2.2 an unnormalized impedance magnitude and phase curve plotted using Balmain's analytical formula is shown to illustrate the parallel (upper hybrid (ω_{uh})) and series (cyclotron (Ω_{ce})) resonances.

However, the concept of a resonance implies that the energy is effectively coupled from the antenna into the plasma. When this occurs the current distribution varies from the traditional triangular current, introducing errors in Balmain's model [1]. In addition, at

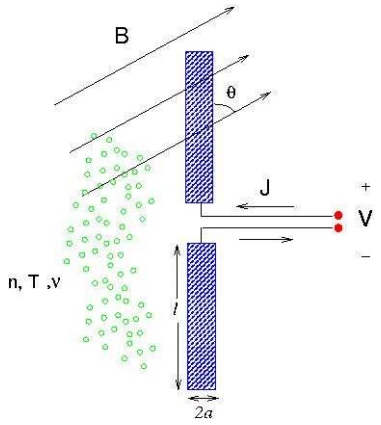

Fig. 2.1: A dipole antenna in plasma showing the feed and orientation with respect to the magnetic field.

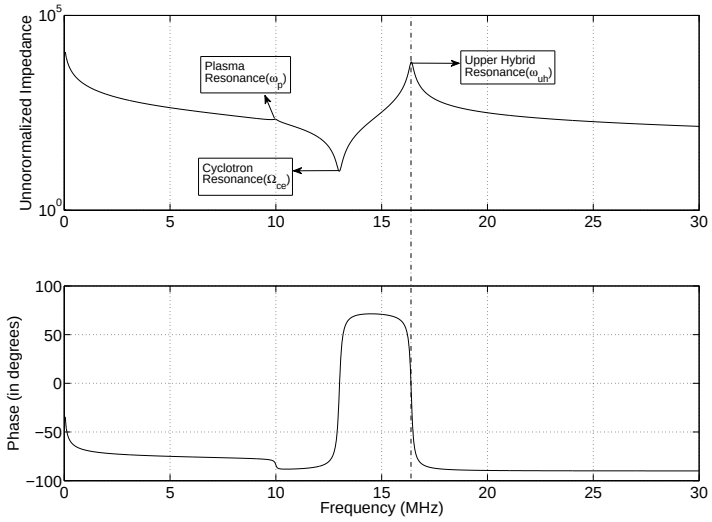

Fig. 2.2: Unnormalized impedance magnitude and phase of a dipole antenna in a cold magnetoplasma using Balmain's formula $Z_B(f)$ showing the key resonance regions and phase transitions.

high frequencies the quasi-static analysis is unable to completely converge to the full wave analysis of Balanis [3].

Major assumptions and limitations of the closed form analytical theories for electrically short antennas immersed in plasma are the following [12]:

1. They are limited to dipole or loop configurations where the assumed current distributions along the antenna is simplified and the resonance effects of the current distribution are assumed to be negligible.

2. This produces a high-frequency plasma model, ignoring any transient behavior and low-frequency behavior where ion dynamics become important.

3. A cold, linear plasma is assumed, where temperature effects and nonlinear shock-like phenomena are neglected.

4. These theories are limited to quasi-static model of the electric fields and magnetic fields, which ignores interactions between the fields and their impact on the antennas impedance.

5. Analytical theories are limited to spatially uniform plasma density distribution, preventing the accurate self-consistent description of plasma sheath effects on antenna impedance.

2.3 Plasma Fluid Finite Difference Time Domain (PF-FDTD) Simulation

The Plasma Fluid Finite Difference Time Domain (PF-FDTD) is an numerical model that incorporates the 5-moment Maxwellian distributed plasma fluid equations with Maxwell's equations in order to understand the physics and electrical properties of an RF source immersed in a plasma environment [1]. The simulation solves for the electromagnetic fields, fluid densities, and fluid velocities for each plasma species around an antenna self-consistently using an explicit leapfrog finite difference time domain scheme originally developed by K. S. Yee [13] and later modified by others [14].

The PF-FDTD model is based upon Maxwell's equations and the 5-Moment Maxwellian fluid equations, with the ideal gas law used to truncate the series:

$$\nabla \times \mathbf{E} = -\frac{\partial \mathbf{B}}{\partial t} , \tag{2.18}$$

$$\nabla \times \mathbf{B} = \epsilon\mu \frac{\partial \mathbf{E}}{\partial t} + \mu \mathbf{J} , \tag{2.19}$$

$$\mathbf{J} = \sum_s q_s n_s \mathbf{u_s} , \tag{2.20}$$

$$\frac{\partial n_s}{\partial t} + \nabla \cdot (n_s \mathbf{u}_s) = \mathbf{P} - \mathbf{L} , \tag{2.21}$$

$$m_s n_s \left(\frac{\partial \mathbf{u}_s}{\partial t} + (\mathbf{u}_s \cdot \nabla)\mathbf{u}_s \right) = n_s q_s (\mathbf{E} + \mathbf{u}_s \times \mathbf{B}) - \nabla P_s - m_s n_s \sum_{\alpha \neq s} \nu_{s\alpha} (\mathbf{u}_s - \mathbf{u}_\alpha) , \tag{2.22}$$

$$P_s = n_s k_b T. \tag{2.23}$$

The antenna is enclosed by a numerical bounding box that provides retarded time absorbing boundary conditions for the electromagnetic field. The electromagnetic fields are numerically solved using the Maxwell curl relations, and each plasma species density n_s and velocity $\mathbf{u}_s$ throughout the computation domain is calculated using the fluid continuity and momentum equations. Ambient density gradients over the extent of the antenna are neglected. The fluid equations are linearized to the first order, to solve only for the electromagnetic and plasma wave disturbances.

The voltage at the antenna terminals is prescribed as one of the inputs to the simulation. A number of voltage sources like dc, sine, sinc, pulse, raised cosine, gaussian, and gaussain derivative can be specified as inputs to the simulation. For multi-frequency analysis a gaussian derivative voltage pulse of sufficient spectral bandwith is fed into the antenna structure. The resulting current at the feed point of the antenna is obtained from the simulation. The impedance of the antenna as shown in fig. 2.3 is then calculated by dividing the Fourier transform of the gaussian derivative voltage input by the Fourier transform of the current through the antenna terminals. The PF-FDTD simulation is performed long enough so that at least five cycles of the lowest frequency of interest is captured.

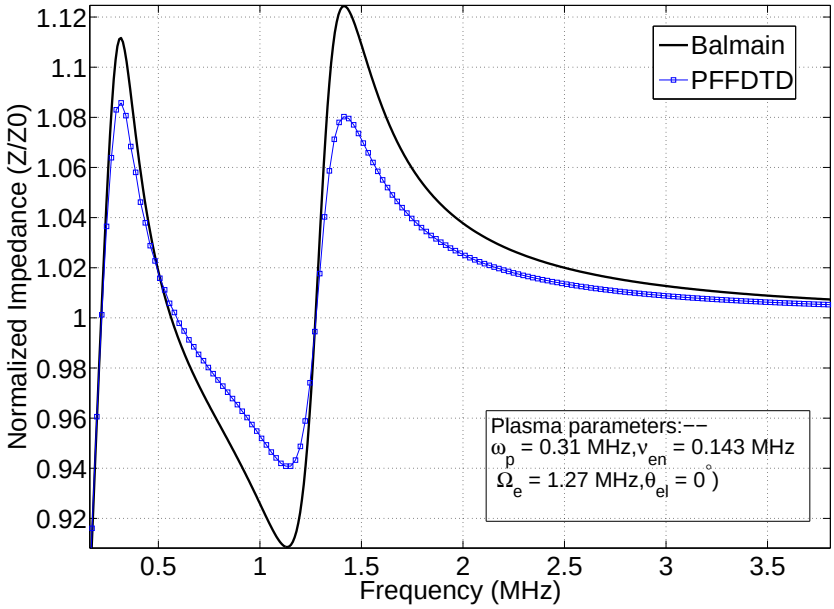

Fig. 2.3: Simulated and theoretical plots of impedance magnitude of a dipole antenna of length 1.04 m and 2.54 cm diameter oriented along the magnetic field. Sheath size is assumed to be zero.

For electrons, the ambient electron density n_{0e}, electron neutral collision frequency ν_{en}, and electron cyclotron frequency f_{ce} are considered to be the variable input parameters for the simulation. For a fixed set of parameters, the impedance magnitudes of a dipole antenna as calculated by the PF-FDTD simulation is compared to the impedance magnitude predicted by Balmain $Z_B(f)$ is shown in fig. 2.3. The minimum impedance is associated with the electron cyclotron resonance frequency f_{ce} and is referred to as the series resonance. At frequencies higher than f_{ce} the maximum impedance observed is associated with the upper hybrid resonant frequency f_{uh} and is called the parallel resonance.

We observe that the resonance positions predicted by the analytical formula $Z_B(f)$ are slightly shifted from that of the PF-FDTD simulation. This difference does not produce serious errors in the values of the parameters f_{pe} and f_{ce}. However, the PF-FDTD impedance curve $Z_{sim}(f)$ predicts a more damped response for the same value of ν_{en}. This difference makes the PF-FDTD a much more accurate tool to obtain the electron neutral collision

frequency. For a match against data, PF-FDTD values of ν_{en} are about 15-20% lower than the values obtained using the analytical formula.

Chapter 3

Electron Density and Electron Neutral Collision Frequency in the Ionosphere Using Plasma Impedance Probe Measurements

3.1 Introduction

The determination of plasma parameters, such as electron density and electron neutral collision frequency, are important for ionospheric plasma characterization. Electron densities and density gradients are used to determine ionospheric plasma properties, while the electron neutral collision frequency ν_{en}, particularly the ratio of the electron neutral collision frequency to the electron cyclotron frequency f_{ce}, is used to determine the dominant ionospheric conductivities and energy conversion processes at different ionospheric latitudes [15].

Radio frequency probe techniques for the determination of plasma parameters are attractive especially because the RF response is not susceptible to spacecraft charging problems at frequencies above the electron plasma frequency [16] where ion sheath effects are negligible. Swept Impedance Probes in dipole configurations have been used on sounding rocket missions [17] to obtain plasma electron densities in the ionospheric E and F layers. Spherical impedance probes have been used in laboratory settings ([18, 19]) under different bias conditions to evaluate absolute electron density. Measurements of dipole antenna impedance in a magnetized plasma with high electron densities (10^7-10^{10} cm^{-3}) and low-collision frequencies have also been reported recently by Blackwell et al. [20].

The Swept Impedance Probe (SIP) measures the small signal RF impedance of an electrically short dipole antenna immersed in a plasma by sweeping a sinusoidal voltage over a range of frequencies and measuring the resulting current at the terminals. The

measured impedance as a function of frequency is characterized by distinct resonant regions that are related to the plasma, electron cyclotron, and the upper hybrid frequencies. These resonant regions are approximately analogous to the resonances of series and parallel RLC circuits. The impedance of the antenna in a plasma is normalized by dividing it with its impedance under free space conditions, which is capacitive at wavelengths much longer than the antenna dimensions.

On the normalized impedance magnitude curve of a dipole antenna immersed in a cold magnetoplasma, the series resonance that occurs near f_{ce} gives the minimum impedance magnitude, while the parallel resonance that occurs near f_{uh} gives a local maximum in the impedance magnitude. The impedance curve for a particular combination of f_{pe}, f_{ce}, and ν_{en} is unique. In a highly ionized, low-collisional plasma, the parallel resonance coincides with a zero crossing in the impedance phase. The determination of the zero crossing has been used in another device known as the Plasma Frequency Probe (PFP) [21]. The PFP uses phase locked loop principles and circuitry to track the zero phase point during sounding rocket missions. This device usually makes use of the same antenna structure as the SIP.

While the measurement technique is fairly well developed ([22,23]), the interpretation of the impedance data poses challenging problems. Identification of the resonant peaks and zero phase location from the impedance curves makes it possible to determine the ambient plasma electron density n_{0e} fairly well. However, the relative height and shape of the series resonance troughs and parallel resonance peaks can be interpreted to determine the electron neutral collision frequency ν_{en}. The measured data is normally compared to analytical formulas for the impedance obtained through mathematical techniques. The most popular analytical theory for a short dipole antenna immersed in a magnetized plasma is that of Balmain [10,11]. The analytical results published by Balmain and others ([7,9,24]) have been used to fit the measured impedance curves with varying degrees of success. The major weakness of the analytical theories are that they do not self-consistently calculate the current distribution along the dipole. This results in the analytical formulas shifting the location of the resonant frequencies slightly, but more importantly, over-estimating the

electron neutral collision frequencies [25].

Nikitin and Swenson [26] argue that the assumed current distribution has very little effect on the general shape of the impedance curve, but do not account for the change in the current distribution near the resonant frequencies [12]. Recently Ward [1] has developed a full-wave plasma-fluid finite-difference time domain electromagnetic code called PF-FDTD that simulates the behavior of a short dipole antenna in a magnetized plasma. The code incorporates the electron continuity and momentum equations to model the plasma environment. The PF-FDTD code computes the current distribution on the antenna structure self-consistently, thus providing a more accurate model for analysis of the measured impedance.

In this work we obtain the absolute electron density and electron neutral collision frequency through analysis of impedance data from the Sudden Atomic Layer (SAL) sounding rocket experiment at different altitudes. The measured data is compared to the analytical formula $Z_B(f)$ of Balmain [11] to obtain initial estimates of n_{0e}, the ambient magnetic field $\mathbf{B_0}$ and ν_{en}. The initial estimates are then used as starting values for the PF-FDTD simulation. The values are then tuned to obtain three numerical fits to the instrument impedance data that yield upper and lower bounds on the derived parameters.

In the next section we give some background of the SAL mission. In sec. 3.3 we describe the SIP instrument and the selected data sets. Following this we present the results of our analysis of the SAL impedance data with the PF-FDTD simulation. In sec. 3.5 we compare our results to those of the standard models. Finally, we draw some conclusions and motivate further work.

3.2 SAL Mission Background

The Sudden Atomic Layer (SAL) sounding rocket was launched from a temporary rocket range at Tortugeuro Beach, Puerto Rico on the evening of February 19, 1998, at 20:09:02 LT. The overall science objective of the SAL rocket mission was in-situ measurement of ionospheric and atmospheric conditions during a sporadic sodium (Na_s) layer event [27]. These Na_s layers are known to be correlated to the sporadic E (E_s) layers. The

rocket flew through a neutral background sodium layer stretching from 80 km to 105 km altitude containing thin Na_s layers at 94 km and 97 km, with peak sodium densities of 6000 cm^{-3} and 4000 cm^{-3}, respectively.

The payload instruments included a charged dust detector to measure mesospheric dust over a mass range of 1000-10,000 amu, a Langmuir probe operating as a Fast Temperature Probe to measure the plasma density and electron temperature, Plasma Impedance (PIP) and DC probes to measure absolute and relative electron densities, electric field booms to measure fields from DC to 5 kHz, telescopes to measure sodium airglow, photometers and lamps to measure sodium and potassium densities, and a positive ion mass spectrometer. Figure 3.1 depicts the payload instrument configuration. At the time of the rocket launch, two ionization layers were present, an intermediate layer at approximately 115 km and an E_s layer at approximately 92.5 km.

We selected three SIP sweeps on the upleg and three on the downleg between 92 to 93 km within the E_s layer to analyze. Although the electron density can be estimated using Balmain's formula for plasma frequencies at 100 kHz and above, these sweeps were selected because the plasma densities were high enough to produce prominent resonance peaks in the impedance magnitude curves and avoid any error in estimation of ν_{en} caused by insufficient coupling at low densities [21].

3.3 Plasma Impedance Probe Instrument and Data

The Plasma Impedance Probe (PIP) in the SAL payload operated in two modes, a Plasma Frequency Probe mode (PFP), and the Swept Impedance Probe mode (SIP). In the SIP mode, the instrument produces an impedance curve by applying a known sinusoidal voltage across the antenna terminals and sweeping across frequencies while measuring the current into the antenna terminals. In the PFP mode, the instrument attempts to lock onto the plasma upper hybrid resonance frequency f_{uh} where the current and the voltage at the antenna terminals are in phase. When locked the PFP provides a measure of the ambient electron density n_{0e} through the relations

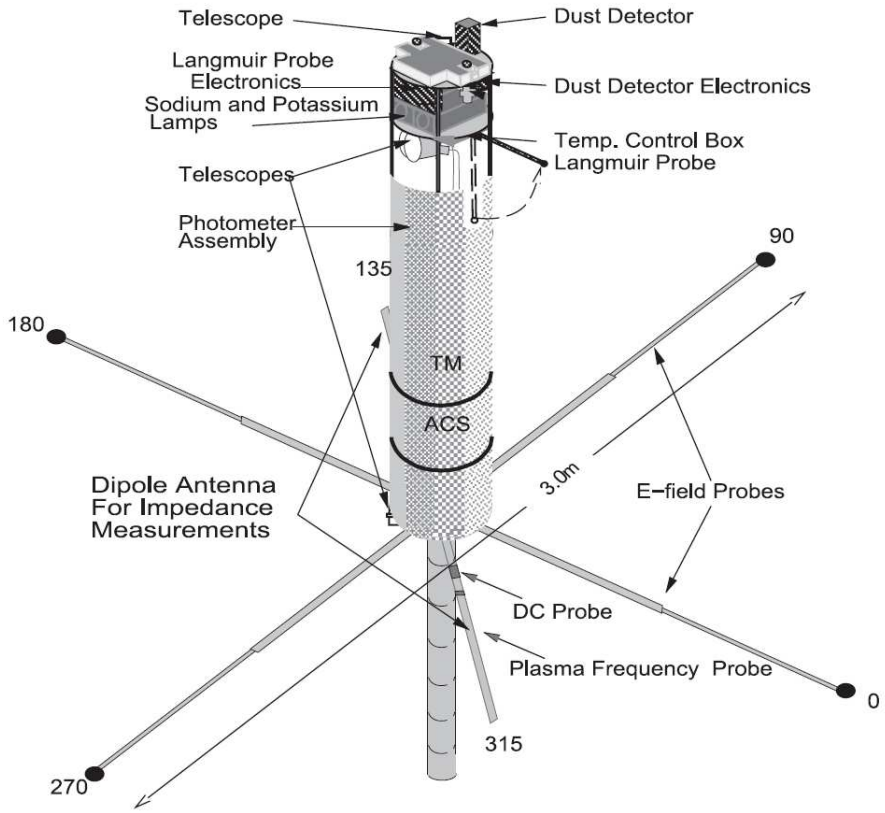

Fig. 3.1: The Sudden Atom Layer (SAL) payload.

$$f_{pe}^2 = f_{uh}^2 - f_{ce}^2 \tag{3.1}$$

$$n_{0e} = \left(\frac{4\pi^2 m_e \epsilon_0}{e^2}\right) f_{pe}^2, \tag{3.2}$$

where e is the electron charge, and m_e is the mass of an electron. The electron cyclotron frequency f_{ce} is derived from magnetometer readings or the International Geomagnetic Reference Field (IGRF) model. The SIP operates as a network analyzer, whereas the PFP is a phase locked loop system that tracks the zero phase point associated with the upper hybrid resonance frequency f_{uh}. The SAL PIP was designed to alternate between the two modes. It could either track the parallel resonance associated with the upper hybrid frequency f_{uh} of the plasma or make sweeping impedance measurements whenever the

phase transition point was undetectable due to very high collisional damping or extremely low plasma densities. The PIP consisted of two booms deployed 180 degrees apart with a 2 m tip-to-tip length and a 2.54 cm diameter. The instrument used the last 52.5 cm of the booms as active elements.

The SIP swept over 40 fixed frequencies starting from 200 kHz to 12 MHz. The frequency resolution of each sweep was 50 kHz from (0.9-1.7) MHz, 100 kHz from (0.2-0.9) MHz and (1.7-2.5) MHz, 500 kHz from (2.5-4.0) MHz, 1 MHz from (4.0-6.0) MHz, and 2 MHz from (6.0-12.0) MHz. The impedance magnitude resolution was approximately 12 Ω over a range of 200 kΩ. During the SAL flight the instrument never switched to the parallel resonance tracking mode (PFP mode), and the dataset consisted entirely of swept impedance magnitude measurements, at the rate of 96 sweeps per second. The response of the plasma surrounding the antenna as a function of frequency was calculated as the ratio of the measured impedance in the plasma regions above 88 km altitude to the averaged impedance at altitudes below 75.5 km where the ionization was negligible.

The selected altitudes for analysis with the PF-FDTD simulation are shown in the plasma frequency profile plots of fig. 3.2 for the upleg and downleg of the flight. The profiles in the figure are proportional to the electron density and were generated following the technique used by Aroh [17]. Balmain's impedance function $Z_B(f)$ was used to find a coarse fit using least mean squares technique against the measured impedance probe data $Z_m(f)$.

$Z_B(f)$ gives the antenna impedance as function of five parameters, f_{pe}, f_{ce}, ν_{en}; the angle with respect to magnetic field θ; and the ion sheath size S. For the coarse fit analysis, only f_{pe} was allowed to vary. The other parameters were estimated using standard reference models. The values of f_{ce} were obtained from the IGRF model. The electron neutral collision frequencies ν_{en} were obtained by using the electron momentum transfer collision frequency formulas from Schunk and Nagy's book [28] and neutral densities from the Mass Spectrometer Incoherent Scatter Radar Extended (MSISE-90) model.

At frequencies higher than the upper hybrid resonance the effects of sheath resonance

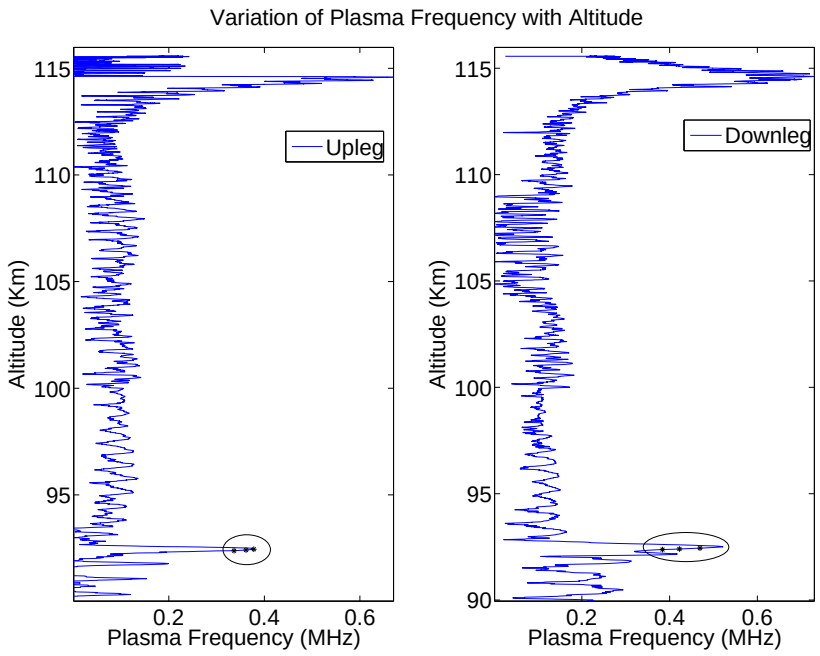

Fig. 3.2: Upleg and downleg plasma frequency profiles obtained through a least square fit of Z_B against Z_m (measured).

and angle to the magnetic field do not play an important role [17], thus θ and S were set to zero for the coarse fit.

From fig. 3.2 we see that the SAL rocket flew through two distinct layers of high plasma density. The modulation in the derived electron density at the rocket spin rate of 1 Hz can also be observed. Three altitudes, 92.37 km, 92.41 km, and 92.44 km, were chosen for the upleg analysis. The selected altitudes are shown in the figure as marks on the altitude profile enclosed by an ellipse. At these altitudes the electron density increases with increasing altitude as can be seen in fig. 3.2.

For the downleg analysis, the three altitudes chosen were 92.38 km, 92.41 km, and 92.44 km. These are also shown in fig. 3.2 enclosed by an ellipse. An upward trend of electron density with increasing altitude is also noted in this case.

3.4 Analysis of Impedance Data

The PF-FDTD software is capable of simulating the behavior of a multi-species plasma,

but here the ions and neutrals have been assumed to be stationary. The multi-fluid equations are particularized to solve only for the perturbed electron density and electron momentum in the computation domain. The simulation includes the pressure gradient $-\nabla p_e = -\nabla(n_e k_b T_e)$, but for ionospheric plasmas in typical rocket missions the cold plasma approximation can be used, so we set $T_e = 0$. Here k_b is the Boltzmann's constant.

The analysis of the impedance data with the PF-FDTD simulation requires that initial estimates for the plasma parameters be determined. These initial parameters f_{pe}, f_{ce} and ν_{en}, were determined by comparing the impedance magnitude data with the analytical formula $Z_B(f)$ using a least square fit algorithm weighted by the confidence level in the instrument measurement over different frequency ranges.

With the starting parameters obtained from $Z_B(f)$, we performed simulation runs to compare the impedance magnitude curves produced by the PF-FDTD simulation $Z_{sim}(f)$ against the rocket impedance magnitude data $Z_m(f)$. The values were tuned until three alternative $Z_{sim}(f)$ fits were obtained to the measured impedance $Z_m(f)$. The three PF-FDTD matched results for each altitude, PF-1, PF-2, and PF-3, are chosen based on confidence in the measured impedance above the upper hybrid resonance frequency.

PF-1 is chosen so that it approximates the lower envelope of the impedance magnitude data slope at frequencies higher than the upper hybrid resonance f_{uh}. PF-2 and PF-3 are chosen so that they approximate the median and the upper envelopes of the measured impedance slope at frequencies higher than the f_{uh}. This method for selection of the impedance curves is repeated for all upleg and downleg impedance data. This was done in order to get reasonable parameter values considering the uncertainty in the impedance data. The measured impedance curve is most reliable above f_{ce}. However, the data has some oscillation as the impedance magnitude curve decays after f_{uh}. Through our selection of upper, median, and lower envelopes, we provide error bounds for values of the plasma parameters.

For all the measurements the dipole was within the payload wake. The current was measured on only one arm of the dipole, which was always in a reasonably homogeneous

plasma. Barjatya and Swenson [17] have shown via a DSMC simulation that on the upleg the density around the SIP should see a minimum reduction by a factor of 1.25. However, the DSMC simulation includes only the neutral particles and a more substantive analysis of the wake structure involving the charged particle effects will be necessary in order to precisely account for the wake effects.

3.4.1 Upleg Analysis

For the upleg, we selected three altitudes in the E_s layer. The three selected heights are 92.37 km, 92.41 km, and 92.44 km. The three altitudes are chosen to be at approximately the same height as those on the downleg. The horizontal rocket velocity was about 350 m/s and the distance between the selected locations is approximately 40 km. The SAL payload was at an angle of 68° with respect to the Earth's magnetic field on the upleg at the height of 92.5 Km [27].

The dipole was oriented perpendicular to the payload, but the spin phase of the rocket could not be reliably determined. Since the angle of the dipole with respect to the magnetic field could vary between 22° to 90° on the upleg, all the simulation runs were done with an elevation angle (θ_{el}) equal to 22°, but the median envelope PF-2 curves were also matched using 90° elevation. This gives us the maximum spread of collision frequency values with the median envelope as a reference.

At the altitude of 92.37 km, the PF-FDTD simulation best fits at elevation angle 22° are shown in fig. 3.3. The parameter values obtained are shown in table 3.1,which also shows plasma parameters obtained from Balmain's theory. The plasma parameters obtained from Balmain's model are obtained under the same matching condition as PF-2. We see that the plasma electron density n_{0e} increases from lower to upper envelopes, with the median envelope giving n_{0e} of 1658 cm^{-3}, which is between the lower and upper envelope n_{0e} values. The electron neutral collision frequency at this height is between 90 kHz to 120 kHz. The collision frequency values obtained from Balmain's theory are much higher than the values of PF-2.

For the other two altitudes, we observe similar trends. The lowest plasma electron

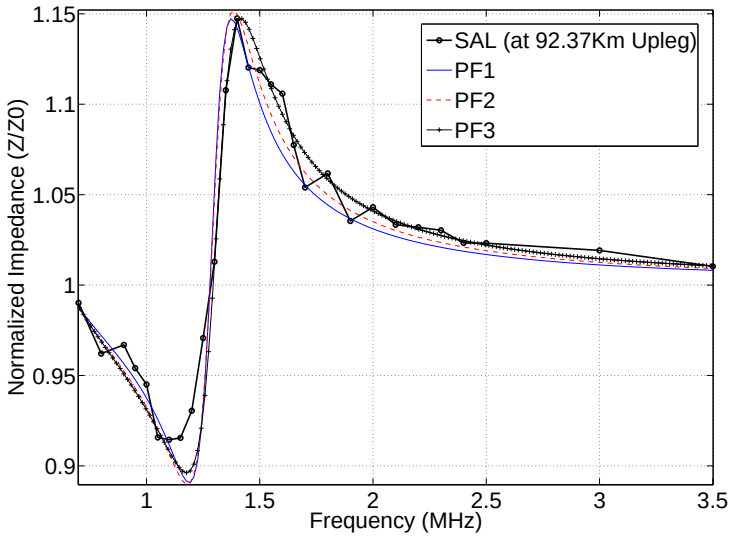

Fig. 3.3: Three PF-FDTD impedance curves matched to SAL impedance data at an altitude of 92.37 km on the upleg.

density (1476 cm^{-3}) was obtained at altitude 92.37 km and the highest (2418 cm^{-3}) at altitude 92.44 km. The impedance curves at 92.41 km and 92.44 km altitudes are shown in figs. 3.4 and 3.5, respectively.

The cyclotron resonance troughs indicate a higher ambient magnetic field than that predicted by IGRF model. The IGRF model predicts a magnetic field of 38,706 nT which corresponds to a cyclotron frequency f_{ce} of 1.06 MHz. If this value is used in $Z_B(f)$ or the PF-FDTD analysis the resultant impedance curves cannot be matched to the measured data. Our analysis yields much higher values of ambient magnetic field strength between 46000 and 47000 nT. This may be due to an additional magnetic field from the Mass Spectrometer which was present on the payload.

Over all three upleg altitudes, the collision frequencies ranged from 90 kHz (lowest value) at 92.38 km altitude to 140 kHz (highest value) at 92.41 km altitude. Using Balmain's theory for comparison against PF-2 yielded collision frequencies between 150 kHz and 170 kHz, while PF-2 values were between 101 kHz and 118 kHz.

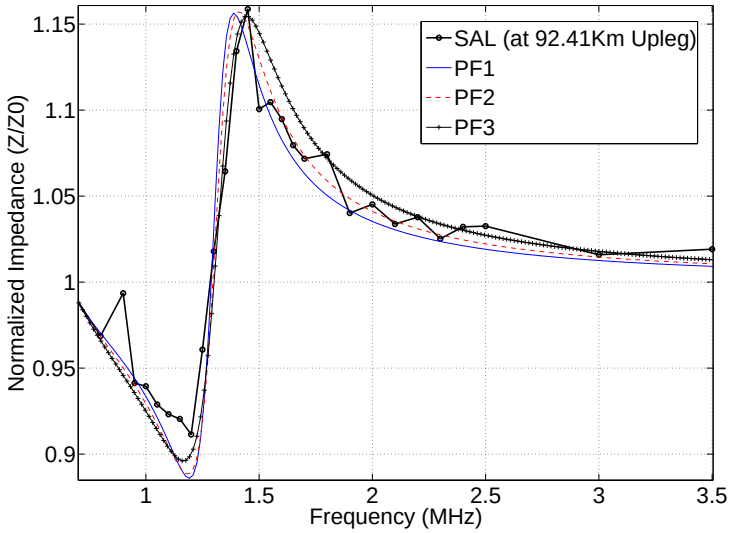

Fig. 3.4: Three PF-FDTD impedance curves matched to SAL impedance data at an altitude of 92.41 km on the upleg.

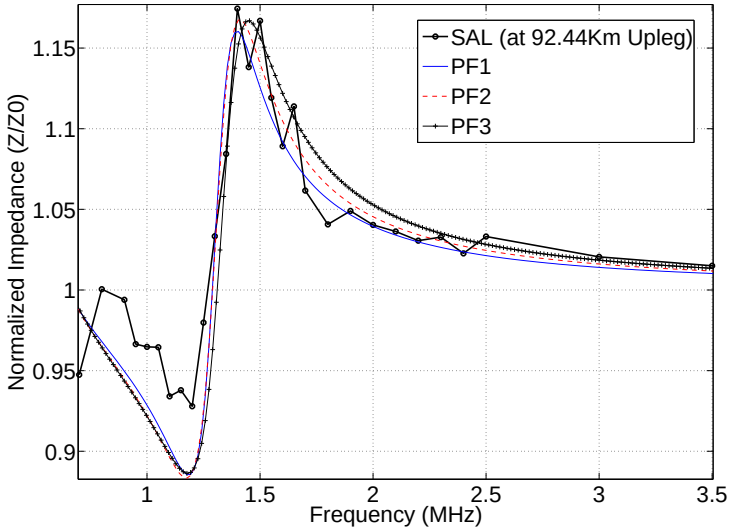

Fig. 3.5: Three PF-FDTD impedance curves matched to SAL impedance data at an altitude of 92.44 km on the upleg.

Table 3.1: Plasma parameters obtained by comparing SAL impedance data on the upleg at an elevation angle θ_{el} 22° against PF-FDTD simulations and Balmain's theory.

Height=92.37 Km, Upleg				
Parameter	PF-1	PF-2	PF-3	Balmain
$f_{pe}(MHz)$	0.34	0.36	0.39	0.35
$f_{ce}(MHz)$	1.27	1.27	1.28	1.27
$\nu_{en}(MHz)$	0.09	0.10	0.12	0.15
$n_{oe}(/cc)$	1476	1658	1917	1552
$B(nT)$	46,355	46,355	46,852	46,374
Height=92.41 Km, Upleg				
Parameter	PF-1	PF-2	PF-3	Balmain
$f_{pe}(MHz)$	0.36	0.39	0.43	0.369
$f_{ce}(MHz)$	1.28	1.28	1.29	1.28
$\nu_{en}(MHz)$	0.10	0.11	0.14	0.17
$n_{oe}(/cc)$	1658	1917	2343	1725
$B(nT)$	46,604	46,852	47,100	46,892
Height=92.44 Km, Upleg				
Parameter	PF-1	PF-2	PF-3	Balmain
$f_{pe}(MHz)$	0.38	0.41	0.44	0.39
$f_{ce}(MHz)$	1.28	1.28	1.30	1.28
$\nu_{en}(MHz)$	0.11	0.12	0.14	0.17
$n_{oe}(/cc)$	1851	2125	2418	1914
$B(nT)$	46,604	46,604	47,352	46,666

3.4.2 Downleg Analysis

The angle of the dipole with respect to the magnetic field varies between 72° to 90° on the downleg. All the simulation runs were done with an elevation angle (θ_{el}) equal to 72°, but the median envelope PF-2 curves were also matched using 90° elevation. This gives us the maximum spread of collision frequency values with the PF-2 curve as a reference.

The plasma parameters obtained with elevation angle 72° are shown in table 3.2,which also shows plasma parameters obtained from Balmain's theory. We note that the ambient magnetic field strengths obtained on the downleg were again much higher than predicted by the IGRF model.

For the downleg altitude of 92.38 km, the PF-FDTD simulation results are shown in fig. 3.6. The impedance curves at 92.41 km and 92.44 km altitudes are shown in figs. 3.7 and

Table 3.2: Plasma parameters obtained by comparing SAL impedance data on the downleg at an elevation angle θ_{el} 72° against PF-FDTD simulations and Balmain's theory.

Height=92.38 Km, Downleg				
Parameter	PF-1	PF-2	PF-3	Balmain
$f_{pe}(MHz)$	0.27	0.31	0.34	0.30
$\nu_{en}(MHz)$	0.07	0.10	0.09	0.16
$n_{oe}(/cc)$	944	1249	1476	1140
$B(nT)$	46,355	46,103	46,355	46,556
Height=92.41 Km, Downleg				
Parameter	PF-1	PF-2	PF-3	Balmain
$f_{pe}(MHz)$	0.35	0.40	0.43	0.34
$\nu_{en}(MHz)$	0.11	0.14	0.16	0.18
$n_{oe}(/cc)$	1596	1986	2343	1430
$B(nT)$	46,852	46,355	46,604	46,764
Height=92.44 Km, Downleg				
Parameter	PF-1	PF-2	PF-3	Balmain
$f_{pe}(MHz)$	0.42	0.44	0.46	0.37
$\nu_{en}(MHz)$	0.11	0.12	0.13	0.17
$n_{oe}(/cc)$	2270	2494	2729	1730
$B(nT)$	46,604	47,352	47,849	47,615

3.8, respectively. As was observed on the upleg, the plasma electron density n_{0e} increases from lower to upper envelopes, with the median envelope giving n_{0e} of 1249 cm^{-3}, which is between the lower and upper envelope n_{0e} values. The electron neutral collision frequency at this height is between 68 kHz to 100 kHz. Higher values of collision frequency are again predicted by Balmain's model when compared with PF-2.

The lowest plasma electron density of 944 cm^{-3} was obtained at altitude 92.38 km and the highest value 2729 cm^{-3} at altitude 92.45 km. Collision frequencies varied from a low of 70 kHz at 92.38 Km to a high of 160 kHz at 92.41 Km. PF-2 collision frequency values varied between 100 kHz and 138 kHz, Balmain's theory in comparison yielded collision frequencies between 156 kHz and 180 kHz.

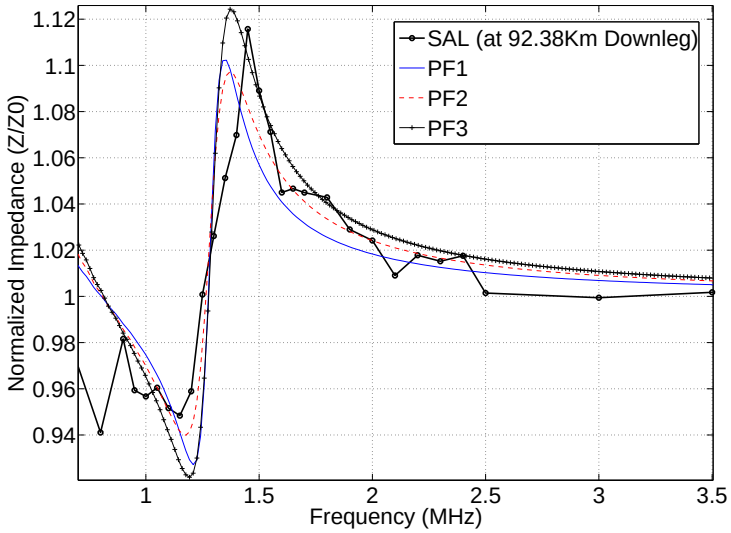

Fig. 3.6: Three PF-FDTD impedance curves matched to SAL impedance data at an altitude of 92.38 km on the downleg.

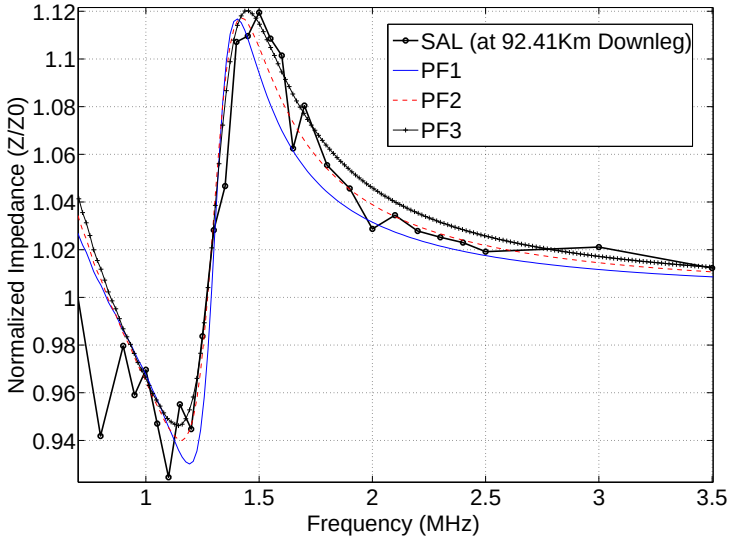

Fig. 3.7: Three PF-FDTD impedance curves matched to SAL impedance data at an altitude of 92.41 km on the downleg.

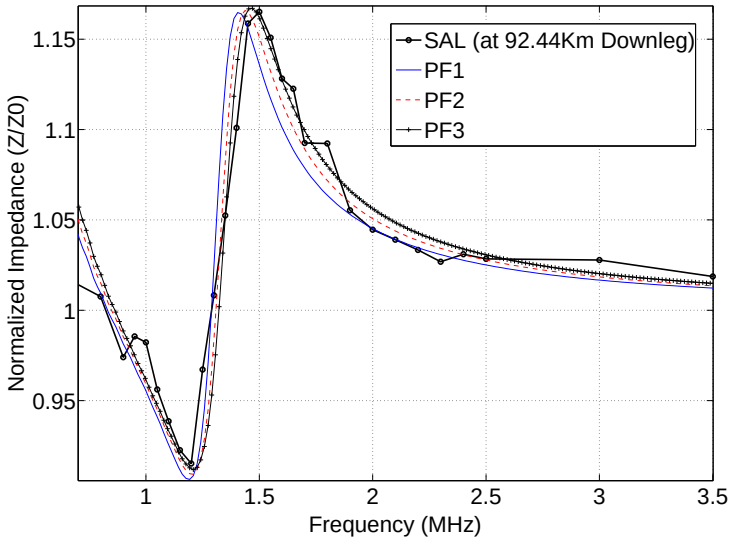

Fig. 3.8: Three PF-FDTD impedance curves matched to SAL impedance data at an altitude of 92.45 km on the downleg.

3.5 Discussion

For a cold collisional fluid plasma the flow of the electrons perpendicular to the magnetic field is given by Cowley [29]:

$$\mathbf{u_{e\perp}} = \frac{1}{1+\left(\frac{\nu_{en}}{2\pi f_{ce}}\right)^2}\left[\frac{\mathbf{E}\times\mathbf{B}}{B^2} - \frac{\nu_{en}}{2\pi f_{ce}}\frac{\mathbf{E}_\perp}{B}\right]. \tag{3.3}$$

Under the same assumptions the field-perpendicular ion flow will have a similar expression. If the ambient density of ions (n_{0i}) is assumed equal to n_{0e} then the current density perpendicular to the magnetic field is given by

$$\begin{aligned} j_\perp &= n_{0e}e(\mathbf{u_{i\perp}} - \mathbf{u_{e\perp}}) \\ &= \sigma_p\mathbf{E} + \sigma_H\mathbf{B}\times\mathbf{E}, \end{aligned} \tag{3.4}$$

where $\mathbf{u_{i\perp}}$ is the field-perpendicular ion flow velocity; σ_p and σ_H are the Pederson and Hall

conductivity. The ratio ν_{en}/f_{ce} is expected to remain small throughout the whole region of the ionosphere where appreciable plasma densities are present (above ∼90 km). Thus electrons should $\mathbf{E} \times \mathbf{B}$ drift at all ionospheric altitudes and contribute only to the Hall current [29]. Further, electron drift along neutral winds is negligible at altitudes between 80-100 km [15].

Electron neutral collisions at 90 - 100 Km are dominated by momentum transfer mechanisms [28]. At an altitude of around 92-95 km the momentum transfer collision frequencies calculated from the Chapman-Cowling collision integral [30] depend strongly on the density of molecular nitrogen(N_2) and oxygen(O_2).

The electron-oxygen and electron-nitrogen collision frequencies with changing density and electron temperature are given by Shunk and Nagy [28],

$$\nu_{N_2} = 2.33 \times 10^{-11} n_{N_2} (1 - 1.21 \times 10^{-4} T_e) T_e, \tag{3.5}$$

$$\nu_{O_2} = 1.82 \times 10^{-10} n_{O_2} (1 + 3.6 \times 10^{-2} \sqrt{T_e}) \sqrt{T_e}, \tag{3.6}$$

where n_{N_2} and n_{O_2} are the molecular nitrogen and oxygen densities, respectively.

We obtain the neutral densities and the electron temperature profiles from the MSISE-90 model, the inputs being the day, time, year, latitude, and longitude of the SAL mission. The MSISE values are then used in eqs. (3.5) and (3.6) to produce an altitude profile for the collision frequencies. To obtain the effective electron neutral collision frequency with altitude, we calculate the weighted average of the two collision frequency profiles according to the expression,

$$\nu_{avg} = \frac{n_{N_2}\nu_{N_2} + n_{O_2}\nu_{O_2}}{n_{N_2} + n_{O_2}}. \tag{3.7}$$

When the densities of the neutral species are almost equal, the weighted average drops down to the arithmetic mean of the two collision frequencies [31]. The altitude profiles shown in fig. 3.9 are generated for electron-nitrogen, electron-oxygen, and weighted average

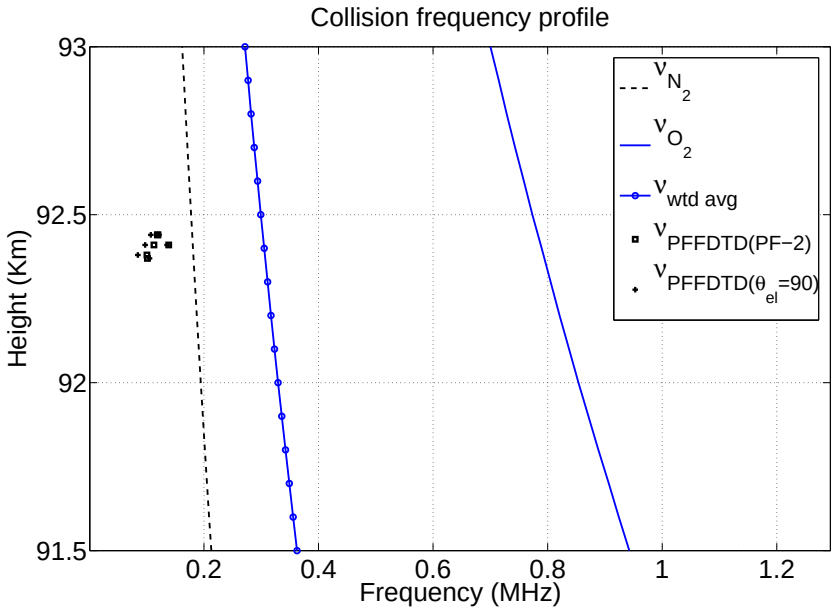

Fig. 3.9: Collision frequencies inferred from PF-FDTD best fits to SAL PIP data plotted along with the theoretical values obtained from Shunk and Nagy's book.

collision frequencies. The collision frequency values obtained from the median envelopes (PF-2) are also shown in fig. 3.9. In addition to the values obtained for the upleg and downleg angles of 22 and 72 degrees, we also show the values obtained with the maximum 90 degree elevation between the dipole and ambient magnetic field. We observe that the collision frequencies using the median envelope (22 and 90 degrees upleg, 72 and 90 degrees downleg) are all within 10 percent of each other at each altitude.

The highest and lowest values obtained from PF-FDTD analysis for the ratio of ν_{en} to f_{ce} (1.06 MHz, obtained from IGRF) are 0.066 and 0.1509, respectively. These numbers are consistent with the assumption that electrons contribute only to the Hall current. We also note that the electron neutral collision frequencies obtained from the PF-FDTD simulation are lower than the collision frequencies derived from the quiet time MSISE-90 neutral densities.

3.6 Conclusions and Future Work

We found that a Swept Impedance Probe can be used to measure the electron neutral

collision frequency and electron density accurately in the vicinity of the probe. The PF-FDTD simulation is a much more powerful tool to estimate the electron fluid parameters than the analytical formulas of Balmain. This is especially true in the case of values of ν_{en}. The electron neutral collision frequency values obtained were more than 20% lower than the values predicted by Balmain's theory.

Since the dipole was within the wake structure of the payload when the measurements were made, a correction factor needs to be determined to obtain the true values of n_{0e} and ν_{en} far away from the payload. In order to do this a more substantive analysis of the wake structure involving the charged particle effects will be necessary. We are currently researching the available techniques to perform this analysis.

Simulation time limits the usage of PF-FDTD to analyzing relatively small data sets. Future work will continue to reduce the simulation time by efficient utilization of memory allocation and parallelizing the finite difference calculations. This will allow the simulation to be used for analyzing the impedance over the entire flight path.

Chapter 4

Algorithm for Automated Data Reduction Using PF-FDTD

One of the biggest limitations of using PF-FDTD for analyzing large data sets is the long simulation time required. Following the suggestions of Ward [1], the scaling property of the linearized code can be used to reduce computational time. This chapter explains the linearized PF-FDTD simulation and why frequency scaling works. This interesting feature of PF-FDTD and Balmain's theory are used in conjunction to develop a matching technique that automates the procedure that was explained in Chapter 3. This simple algorithm will allow the PF-FDTD simulation to be used for analyzing impedance data at a larger set of altitudes over the entire flight trajectory.

4.1 The Linear Fluid Model and Frequency-Scaling

Assuming the inertial term in the momentum equation $((\mathbf{u}_s \cdot \nabla)\mathbf{u}_s)$ to be small and no production and loss terms, eqs. (2.18-2.22) can be linearized using the perturbative expansion technique. In so doing, it becomes possible to rewrite the field values, by separating the various fields into a DC term and a small time varying component

$$\mathbf{E} = \mathbf{E}_0 + \mathbf{E}_1 \ , \tag{4.1}$$

$$\mathbf{B} = \mathbf{B}_0 + \mathbf{B}_1 \ , \tag{4.2}$$

$$\mathbf{u}_s = \mathbf{u}_{0_s} + \mathbf{u}_{1_s} \ , \tag{4.3}$$

$$n_s = n_{0_s} + n_{1_s} \ . \tag{4.4}$$

The constant electric field is assumed to be zero. Once the field values are separated into constant and small perturbation terms, the fundamental eqs. (2.18-2.22) become,

$$\nabla \times \mathbf{E_1} = -\frac{\partial \mathbf{B_1}}{\partial t} , \tag{4.5}$$

$$\nabla \times \mathbf{B_1} = \epsilon\mu\frac{\partial \mathbf{E_1}}{\partial t} + \mu\sum_s q_s(n_{0_s}\mathbf{u}_{0_s} + n_{1_s}\mathbf{u}_{0_s} + n_{0_s}\mathbf{u}_{1_s}) , \tag{4.6}$$

$$0 = \frac{\partial n_{1_s}}{\partial t} + \nabla \cdot (n_{1_s}\mathbf{u}_{0_s} + n_{0_s}\mathbf{u}_{1_s}) , \tag{4.7}$$

$$\begin{aligned} m_s n_{0_s}\left(\frac{\partial \mathbf{u}_{1_s}}{\partial t}\right) = {} & q_s n_{0_s}(\mathbf{E_1} + \mathbf{u}_{1_s} \times \mathbf{B_0} + \mathbf{U}_{0_s} \times \mathbf{B_1}) \\ & + q_s(n_{0_s} + n_{1_s})(\mathbf{u}_{0_s} \times \mathbf{B_0}) - k_b T \nabla n_{1_s} \\ & - m_s(n_{0_s} + n_{1_s})\sum_{\alpha \neq s}\nu_{s\alpha}(\mathbf{u}_{0_s} - \mathbf{u}_{0_\alpha}) \\ & - m_s n_{0_s}\sum_{\alpha \neq s}\nu_{s\alpha}(\mathbf{u}_{1_s} - \mathbf{u}_{1_\alpha}) . \end{aligned} \tag{4.8}$$

For the cases considered here a non-flowing cold plasma ($\mathbf{u}_{0_s} = 0$ and $T = 0$) has been assumed and the equations are only solved for electrons. Thus the equations that are solved by PF-FDTD simulation reduce to:

$$\nabla \times \mathbf{E} = -\frac{\partial \mathbf{B}}{\partial t}, \tag{4.9}$$

$$\nabla \times \mathbf{B} = \epsilon_0\mu_0\frac{\partial \mathbf{E}}{\partial t} + \mu_0 \mathbf{q}_e n_{0e}\mathbf{u}_e, \tag{4.10}$$

$$\frac{\partial n_e}{\partial t} = -n_{0e}(\nabla \cdot \mathbf{u}_e), \tag{4.11}$$

$$m_e n_{0e}\frac{\partial \mathbf{u}_e}{\partial t} = n_{0e}q_e(\mathbf{E} + \mathbf{u}_e \times \mathbf{B}_0) - n_{0e}m_e\nu_{en}\mathbf{u}_e, \tag{4.12}$$

where n_{0e} is the background density, n_e is the first order density variation, $\mathbf{u}_e$ is the first order velocity perturbation (the subscript 1 has been dropped from all the first order perturbation terms), and ν_{en} is the electron neutral collision frequency. The ambient magnetic field strength is given by $\mathbf{B}_0$.

For harmonic plane wave solutions, the differential operators ∇ and $\partial/\partial t$ are replaced by $j\mathbf{k}$ and $-j\omega$ respectively, so that the differential equations become simple algebraic

equations. Therefore, eqs. (4.9, 4.10, 4.12) can be written as:

$$\mathbf{k} \times \mathbf{E} = -\omega \mathbf{B}, \tag{4.13}$$

$$j\mathbf{k} \times \mathbf{B} = \mu_o(-en_{0e}\mathbf{u}_e) - \frac{1}{c^2} j\omega \mathbf{E}, \tag{4.14}$$

$$-j\omega m_e \mathbf{u}_e = -e(\mathbf{E} + \mathbf{u}_e \times \mathbf{B}_o) - m_e \nu_{en} \mathbf{u}_e. \tag{4.15}$$

The dispersion relation for this case can be derived from the coupled set of eqs. (4.13, 4.14, 4.15). Combining (4.14) and (4.15), and rearranging this set, reduces to

$$\mathbf{k} \times (\mathbf{k} \times \mathbf{E}) + \frac{\omega^2}{c^2}\mathbf{E} = \frac{j\omega e n_{0e}}{\epsilon_0 c^2}\mathbf{u}_e, \tag{4.16}$$

$$\left(1 + j\frac{\nu_{en}}{\omega}\right)\mathbf{u}_e + \frac{ie}{m_e\omega}(\mathbf{u}_e \times \mathbf{B}_0) = -\frac{je}{m_e\omega}\mathbf{E}. \tag{4.17}$$

Defining the following variables:

$$U = 1 + i\frac{\nu}{\omega}, \tag{4.18}$$

$$Y = \frac{\Omega_{ce}}{\omega}, \tag{4.19}$$

$$X = \frac{\omega_{pe}^2}{\omega^2}, \tag{4.20}$$

$$S = 1 - \frac{XU}{U^2 - Y2}, \tag{4.21}$$

$$D = -\frac{XY}{U^2 - Y^2}, \tag{4.22}$$

$$P = 1 - \frac{X}{U}, \tag{4.23}$$

and using the co-ordinate system and steps explained by Bittencourt [32], it can be easily shown that eqs. 4.16 and 4.17 reduce to the following matrix representation of the the electric field vector:

$$\begin{bmatrix} (S - \eta^2 cos^2\theta) & -jD & \eta^2 sin\theta cos\theta \\ jD & (S - \eta^2) & 0 \\ \eta^2 sin\theta cos\theta & 0 & (P - \eta^2 sin^2\theta) \end{bmatrix} \begin{bmatrix} E_x \\ E_y \\ E_z \end{bmatrix} = 0, \tag{4.24}$$

where the quantity $\eta = (kc/\omega)$ represents the index of refraction of the medium.

The PF-FDTD simulation is generally performed long enough so that at least five cycles of the lowest frequency of interest, which in most cases is the plasma frequency, is captured. The time step of the simulation is fixed by the ratio $dx/2c$ fixed to satisfy the stability conditions. Hence for fixed spatial stepsize dx, the time step would also be fixed. Hence, the time taken for five cycles at the plasma frequency depend inversely on the plasma frequency. In low density plasmas, to properly resolve the low-frequency plasma features, the simulation time needs to be increased proportionately. A set of impedance curves for different plasma frequencies keeping the ratio of collision frequency to plasma frequency and gyro frequency to plasma frequency constant, are shown in fig. 4.1.

Figure 4.2 shows all the impedance curves of fig. 4.1 scaled to the 5 MHz plasma frequency ($\omega_p = 5MHz$) case. It can be clearly seen that the impedance of the dipole antenna scales as long as a constant ratio between all the fundamental frequencies is maintained. This scaling property can be explained by looking closely at eq. (4.24). All elements in the matrix are either constants or dependent on U, Y, and X which themselves are dependent on the ratios of the fundamental frequencies in the plasma. If all the fundamental plasma parameters and the frequency of observation are scaled by a constant factor (i.e., $\omega \rightarrow \lambda\omega$), the U, Y, and X terms remain unchanged, hence the same features are expected in the impedance. This property of the linearized PF-FDTD simulation can be used to reduce the simulation time drastically.

It was observed that for the constant relations between the fundamental frequencies given in eq. (4.25), for $\omega_{pe} = 20$ MHz the first antenna resonance (at high frequencies where the antenna is no longer electrically short) does not affect the impedance at lower frequencies.

$$\frac{\Omega_{ce}}{\omega_{pe}} = 1.5, \qquad \frac{\nu_{en}}{\omega_{pe}} = 0.15 \tag{4.25}$$

The code has not been verified for the antenna frequencies (frequencies where the antenna can no longer be considered as electrically short), hence it is advisable to keep the

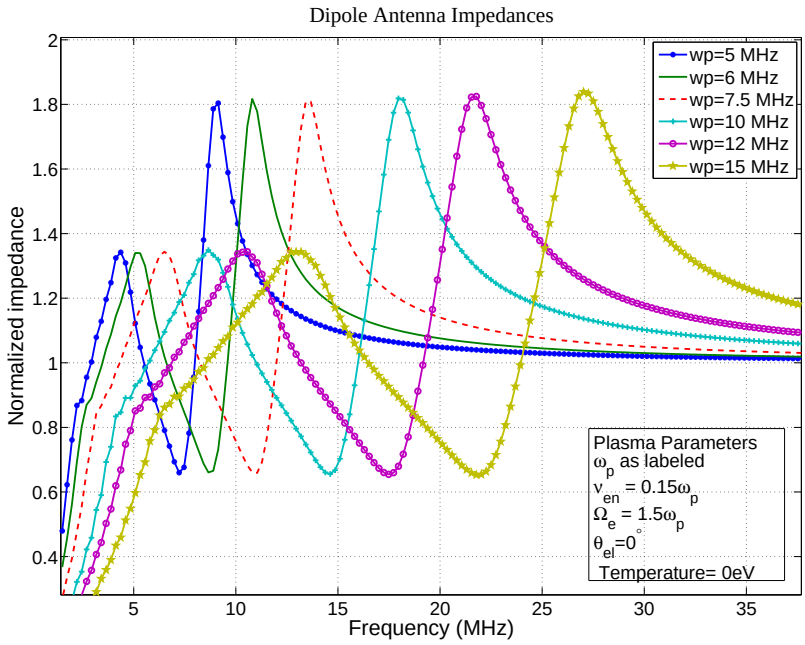

Fig. 4.1: A set of impedance curves for different plasma frequencies simulated by PF-FDTD.

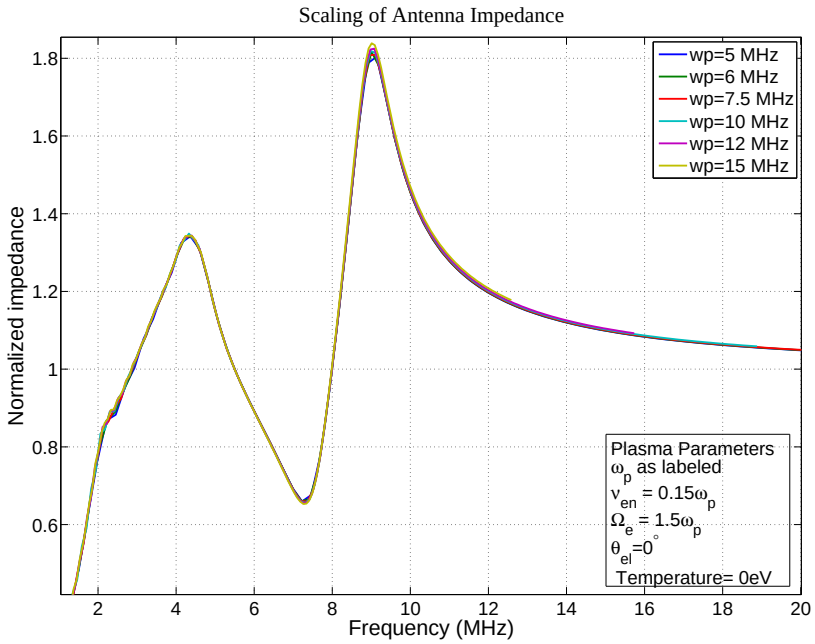

Fig. 4.2: Normalized impedance curves for different plasma frequencies as simulated by PF-FDTD showing the scaling property observed at plasma frequency $\omega_{pe} = 5MHz$.

simulation operating ranges lower than the first antenna resonance frequency.

4.2 Algorithm for Plasma Parameter Extraction

Using the scaling property explained above and an approximate relationship between the balmain parameters and the PF-FDTD parameters, we can automate the entire matching process of Chapter 3. The only inputs to the system are the normalized impedance data from the PIP instrument. Using appropriate matching conditions (upper bound, lower bound, or the median) for both Balmain and PF-FDTD, a few generic steps can be used, as illustrated in the following algorithm to extract the plasma parameters from any set of impedance data.

Algorithm:

Inputs: Normalized Impedance data

Outputs: ω_{pe}, Ω_{ce} and ν_{en}

for i= 1:length of sweeps

Balmain Matching

1. Select a matching criterion (Only slope from ω_{uh} and higher, entire curve, a weighted combination of both).

2. Use any evolutionary algorithm to match Balmain's analytical formula to impedance data.

3. Save Balmain best-fit plasma parameters.

PF-FDTD Matching

1. Set plasma parameter ranges using the Balmain best-fit plasma parameter values.

2. Scale the frequency of operation to reduce computational time.

3. Select a matching criterion (Only slope from ω_{uh} and higher, entire curve, a weighted combination of both).

4. Use evolutionary algorithm to find the best fit.

Note: Use as few PF-FDTD cases as possible to match. The possible range of values has already been reduced by the balmain best fit values.

5. Save best values of plasma parameters.

end

Use of Balmain's analytical formula as part of the matching procedure is essential as it limits the range of possible values of plasma parameters. Although there has not been a formal study to establish an empirical relation between plasma parameters for similar normalized impedance values for Balmain's analytical formula and PF-FDTD, it has been found during the course of this study that the following relations hold for most cases:

$$\omega_{pe_{PF-FDTD}} = (1.05 - 1.23) \times \omega_{pe_{Balmain}}, \tag{4.26}$$

$$\Omega_{ce_{PF-FDTD}} \approx \Omega_{ce_{Balmain}}, \tag{4.27}$$

$$\nu_{en_{PF-FDTD}} = (0.6 - 0.9) \times \nu_{en_{Balmain}}. \tag{4.28}$$

Using these empirical relationships and following the above algorithm reasonably good results have been obtained with as few as eight cases of PF-FDTD for matching against a single impedance curve.

Chapter 5

Aerodynamic Influence on Plasma Impedance Probe Measurements on Sounding Rocket Missions

5.1 Introduction

Sounding rockets remain one of the most popular means of in-situ measurements in the Earth's ionosphere. The ionospheric D, E, and F regions are inaccessible by the conventional means like balloons and satellites, as they are higher than the maximum altitudes attained by balloons and are too low for satellites. Sounding rockets provide means of in-situ measurement in these regions. The Plasma Impedance Probe (PIP) is an RF instrument that is used to measure plasma electron density and electron neutral collision frequency. Radio Frequency probe techniques for the determination of plasma parameters are attractive especially because the RF response is not susceptible to spacecraft charging problems at frequencies above the electron plasma frequency where ion sheath effects are negligible [16]. Swept Impedance Probes (SIP) in dipole configurations have been used on sounding rocket missions to obtain plasma electron densities in the ionospheric E and F layers [17, 27].

The wake in the neutral atmosphere around a sounding rocket at mesospheric altitudes is well known and its perturbing effects on in situ measurements have to be taken into account. The effect of spacecraft aerodynamics on many instrument is well documented [33–35]. Any sounding rocket traveling through the ionosphere disturbs the ambient ionospheric environment, and hence introduces errors in measurement. PIP measurements are also affected by the spacecraft aerodynamics. The most common effect seen in the density measurement is the spin modulation observed at the rocket spin rate. This arises due to the fact that the neutral wake perturbs the plasma environment through strong collisional coupling such that data from radially mounted probes spinning through this wake show

spin modulation [17].

Density measurements inferred from PIP data can be made suitable for analysis if the aerodynamic effects are properly quantified and corrected. Numerical simulations of the 3-D steady state external flow field surrounding the spacecraft can be employed to quantify these effects and to infer correction coefficients. In this work we develop a methodology to obtain coefficients to demodulate the spin modulation observed on the electron density measurements by the impedance probes.

In the next section, we discuss how impedance measurements can be affected on a typical sounding rocket mission with particular emphasis on the Sudden Atomic Layer (SAL) mission. Following this in sec. 5.3, we explain some of the tools that have been used for the flow field simulation and also explain the modifications that have been made to the Plasma Fluid Finite Difference Time Domain (PF-FDTD) model of Ward [12] to include the effect of inhomogeneous plasma. Finally, we analyze the results and draw some conclusions.

5.2 Impedance Probe Measurement on a Sounding Rocket

The most popular antenna geometries that are employed as impedance probes are the dipole and monopole. Patch and spherical antennas have also been considered as probes [1, 19]. The probes are generally placed on the sides of the spacecraft (either on booms or on the spacecraft surface itself). The rocket creates a ram side compression and leaves a wake behind it as it moves through the atmosphere. Almost all the measurement on the sounding rocket are affected by being present inside the flow fields of the spacecraft. The most visible effect that is observed on most density measurements when the instrument is within an asymmetric structure is spin modulation of the observed density parameter as the instrument rotates in and out of regions of successive low and high density regions.

If the rocket flight trajectory and orientations are known throughout the flight duration then the aerodynamic effects can be quantified. The wake structure around a spacecraft depends on the angle of attack, the geometry of the spacecraft, and the ionospheric conditions encountered at any particular location. The wake is therefore time dependent, but is

normally assumed to be slow enough on the time scales of the measurement so that we may take snapshots of steady flow around the spacecraft at different instances to obtain a good representation of the flow. Transient effects are therefore neglected for most applications.

The SAL rocket reached an maximum altitude of 115 Km. It was at an angle of 2° to the ram on the upleg and 8° to the ram on the downleg at an altitude of 92.5 km. Direct Simulation Monte-Carlo (DSMC) [36] was used to simulate the flow structures encountered during the SAL mission by Barjatya and Swenson [17]. Figure 5.1 shows results of the DSMC simulation at an altitude of 92.5 km for both upleg and downleg of the SAL mission. An asymmetric wake structure due to the angle of attack is clearly visible.

The rocket used during the SAL mission was spinning at a constant rate of 1 Hz, this spin modulation is observed in the density measurements [17]. The spin modulation observed during SAL mission on electron plasma frequency which is proportional to the electron density measurements, is shown in fig. 5.2. The amplitude spectrum of the plasma frequency shown in fig. 5.3 confirms the fundamental spin rate of the rocket at 1 Hz. The measurements of the instrument must therefore be analyzed post flight to remove the spin modulation effect. It has been reported earlier by Kurihara [37] that the background density is not always obtained by a running average smoothing of the spin modulation observed with side-looking instruments. It is not advisable to average data from fast moving sounding rockets as the averaging is done over physical layers which would lead to loss of information. The accuracy of these measurements can be improved by simulating the actual flow structures around the rocket and subtracting the perturbations introduced due to it.

5.3 Numerical Codes for Studying Wake Structure Effects

The ionospheric neutral densities generally reduces gradually as the altitude increases and a rocket flying through the ionosphere would encounter different flow regimes during its course of flight. The mean free path λ_{mfp} for the neutral molecules determines the Knudsen number, K_n, which is a measure of the flow regime around an object of characteristic length L_c, through the relation [38]:

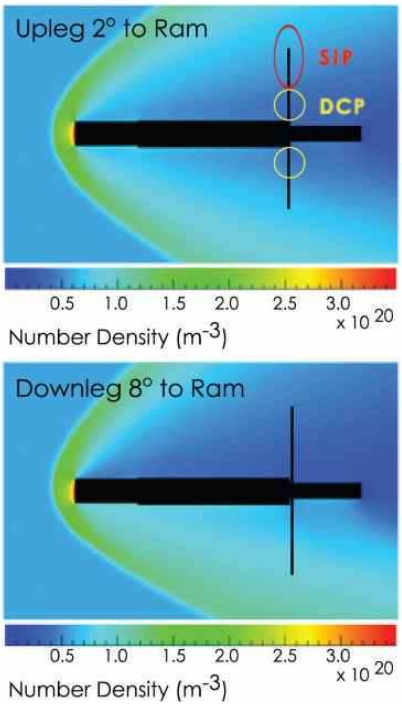

Fig. 5.1: DSMC simulation of the flow structures encountered during the SAL mission at an altitude of 92.5 km on both upleg and downleg. The position of the booms carrying the SIP and DCP with respect to the rocket is shown.

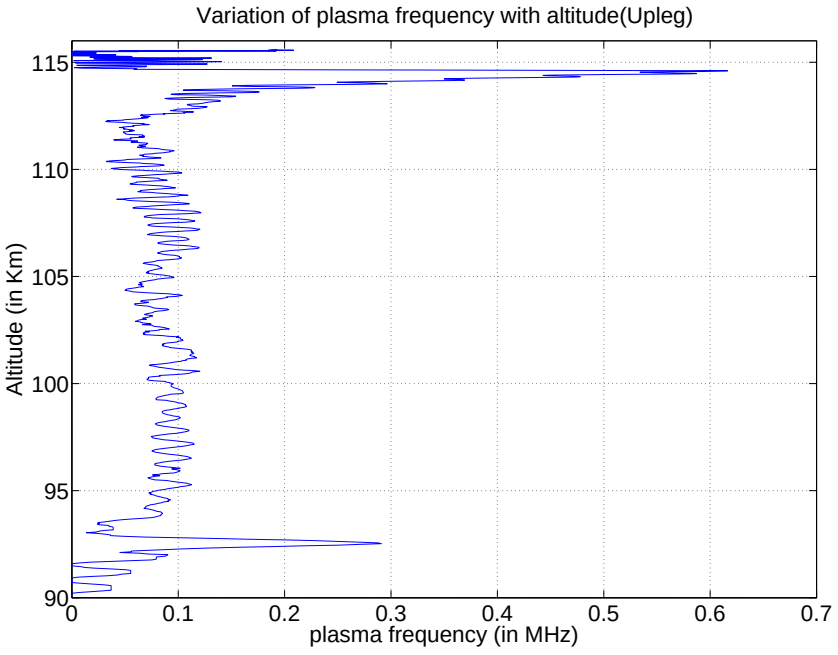

Fig. 5.2: Observed plasma frequencies during the upleg of the SAL mission.

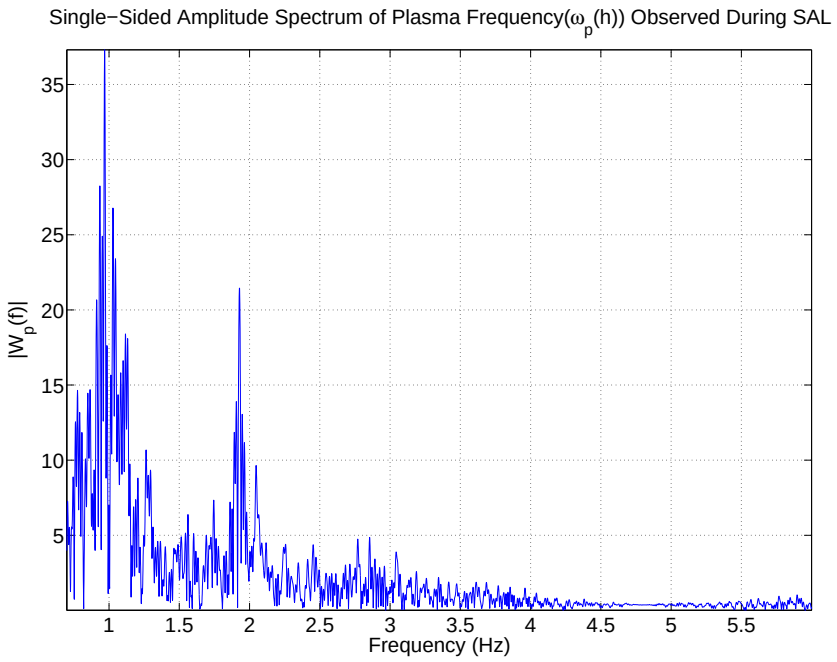

Fig. 5.3: Fourier decomposition of the plasma frequency observed during SAL mission showing the fundamental spin rate of the rocket.

$$K_n = \frac{\lambda_{mfp}}{L_c}. \tag{5.1}$$

5.3.1 DSMC

When K_n is much less than 1, the flow is considered a continuum flow, and can be handled with the usual Navier-Stokes equations of fluid mechanics. At low gas densities the Navier-Stokes equations do not provide a valid model for gases, and errors associated with conventional CFD methods increase as the Knudsen numbers exceed 0.1 [39]. When K_n is much larger than 1, the flow is called a rarefied flow, and particle type calculations such as DSMC has to be employed to simulate the flow. When K_n is around 1, the flow is transitional. For the neutral ionosphere, $K_n = 1$ occurs between 100 to 110 km [37]. The fall off above 110 km is rapid, fig. 5.4 illustrates these steep changes by comparing DSMC simulations of a rocket flying through the ionosphere at 90 km and 100 km above Puerta Rico, neutral density values were obtained from the MSISE-90 model. The DSMC

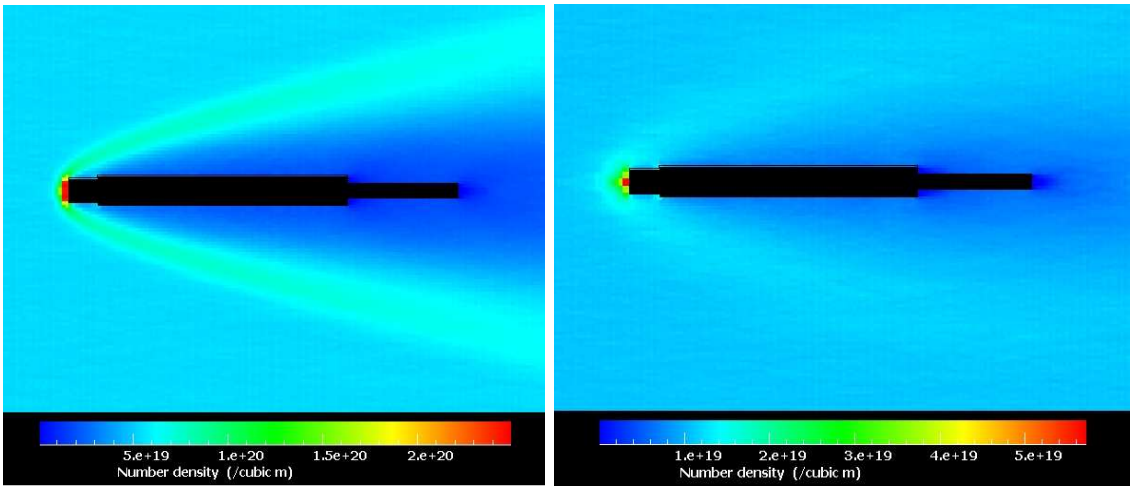

Fig. 5.4: Left panel shows DSMC simulation showing a representative flow around a sounding rocket at an altitude of 90 Km above Puerto Rico . Right panel shows the flow at 100 Km.

method introduced by Bird provides a powerful numerical tool for the analysis of rarefied flows. Basic ideas have been presented comprehensively by Bird [36]. DSMC is a microscopic approach which describes the fate of individual gas molecules under the influence of collisions and boundary interactions with payload surfaces. Macroscopic flow properties like density, temperature, and velocity fields are obtained as appropriate averages by tracing the paths and the interactions of representative molecules. The only inputs are the properties of the undisturbed gas flow (e.g., the number density, temperature, and mean flow velocity) and the relevant properties of the payload (e.g., the geometry, surface temperature, and reflection properties).

The DSMC model can be used for many flow regimes encountered in space which meet its assumed approximations. One of them being that the interaction between the particles can be modeled by collisions. The errors introduced by the various approximations can be minimized if three conditions are fulfilled:

1. The system should be in the collisional regime.

2. The mean free path should be larger than the cell size.

3. The mean time between two collisions should be larger than the time step.

5.3.2 Particle In Cell (PIC)

The ionization rate increases above 110 km at a substantial rate, through the E and F layers. At high Knudsen numbers ($K_n >> 1$), as found at altitudes above 500 km collisions between particles become rare, the ionization is strong and the neutral density low enough that the resulting plasma can be considered almost collisionless. The magnetic field of the Earth is strong enough up to 1000 km so that the plasma is magnetized. As any spacecraft moves through the ionospheric plasma, the collection of charged particles primarily on the ram surfaces will lead to spacecraft charging. This phenomenon will modify the wake structure around the spacecraft. Taking the changing wake structure into account due to charging is further complicated by the presence of charged dust particles found in the ionosphere. Barjatya and Swenson [17] have shown that triboelectric charging in dust layers leads to higher than expected spacecraft potentials. To correct for the modified flow due to spacecraft charging, the gradual change in the charged particle density as the spacecraft goes above 80 km and higher needs to be taken into account.

At higher altitudes, a Particle In Cell (PIC) simulation needs to be used to simulate the flow that accounts for spacecraft charging as well. The Spacecraft Plasma Interaction System (SPIS) software is one such simulation that uses electrostatic 3-D unstructured Particle-In-Cell plasma model to simulate the movement of particles in collisionless plasmas. SPIS model has already been used to simulate spacecraft charging on a suborbital spacecraft [40] and studying the wake formation behind positively charged spacecraft in flowing tenuous plasmas [35]. SPIS models the plasma as a matter-field coupling. Two types of matter models are intergrated in SPIS, the PIC model with linear weighted charge distribution and a global Maxwell-Boltzmann distribution. In PIC model the motion of macroparticles is traced under the influence of electric and magnetic fields. A macro particle constitutes a large number of real particles, whose population is limited by the nominal plasma density.

The resultant flow profile obtained from simulations like DSMC and PIC can be incorporated in the PF-FDTD simulation to study their effects on impedance of antennas.

5.3.3 PF-FDTD for Inhomogeneous Plasma

A multi-species Plasma-Fluid Finite Difference Time Domain Simulation of an antenna immersed in a plasma has been developed at Utah State University under a NASA Grant (NAG5-13026) [1]. The PF-FDTD software simulates the behavior of a multi-species plasma. The multi-fluid equations are particularized to solve only for the perturbed electron density and electron momentum in the computation domain.

The linearized fluid momentum and continuity equations that are analyzed in the PF-FDTD simulation are given by:

$$\frac{\partial n_e}{\partial t} = -n_{0e}(\nabla \cdot \mathbf{u}_e), \tag{5.2}$$

$$m_e n_{0e} \frac{\partial \mathbf{u}_e}{\partial t} = n_{0e} q_e(\mathbf{E} + \mathbf{u}_e \times \mathbf{B}_0) - n_{0e} m_e \nu_{en} \mathbf{u}_e, \tag{5.3}$$

where, n_{0e} is the background density, n_e is the first order density variation, u_e is the first order velocity perturbation, and ν_{en} is the electron neutral collision frequency. These two equations for the electron species fluid are supplemented by the Maxwell equations.

To study the effects of steady state flow fields structure on the impedance, the constant homogeneous background density is modified. The background density is initialized to an inhomogeneous flow structure that is derived either from an approximated or simulated aerodynamic structure. The simulation includes the pressure gradient $-\nabla p_e = -\nabla(n_e k_b T_e)$ term in the momentum equation, but for ionospheric plasmas observed during typical sounding rocket missions electron and ion temperatures are low, and hence the plasma can be treated as cold plasma. Throughout this study electron temperature has been set to zero ($T_e = 0$) for all PF-FDTD simulations. Figure 5.5 shows typical mid-latitude daytime and nighttime temperature for electrons, ions, and neutrals during solar maximum and minimum conditions. The data was generated using the Inter- national Reference Ionosphere (IRI) model calculated over Logan, Utah (Lat. 41 44' 7", Lon. -111 50' 3") by Aroh [41]. It can be clearly seen that the temperature values are much smaller 1 eV ($1eV \approx 11604K$).

Cold plasma assumption makes the effect of density gradient negligible (assumed zero in the analysis). If the cold plasma approximation holds then the term $k_B T_e \nabla n_e$ for the

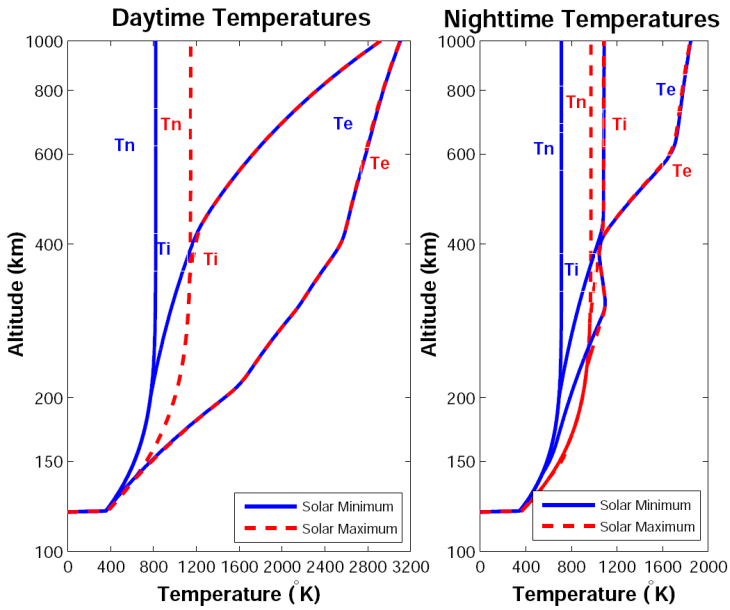

Fig. 5.5: Typical mid-latitude neutral (T_n), ion (T_i), and electron temperature (T_e) profiles.

first order perturbations drops out due to T_e being very small. This makes it possible to drop the pressure gradient in the simulation. Note that the larger variation in density with altitude is not considered as typically a single sweep is performed over only 3-10 meters. Since the RF impedance is only affected by local density gradients, we can neglect them as long as a single sweep is performed fast enough. Preliminary simulations with temperatures in the range 0-100 eV were made to observe the effects of temperture on dipole impedance, but no significant changes in the resonant peak locations for $T_e < 1eV$ was observed. The results of the simulations are shown in fig. 5.6; it can be seen that electron temperature only starts to a play a significant role for energies higher than 5eV which is much higher than the temperatures observed in the ionosphere ($T_e << 1eV$).

The modified code is tested using a test environment of two separate plasmas of different densities with the dipole sitting at the boundary separating the two regions, with one dipole arm in each. The test plasma density environment inside the simulation box of $70 \times 70 \times 65$ cells is shown in fig. 5.7; the orthogonal slice planes through the volumetric data in the simulation box are displayed to show the 3-D distribution of density. The resultant impedance curves for a dipole of length 1.04 m and diameter 0.04 m (antenna is

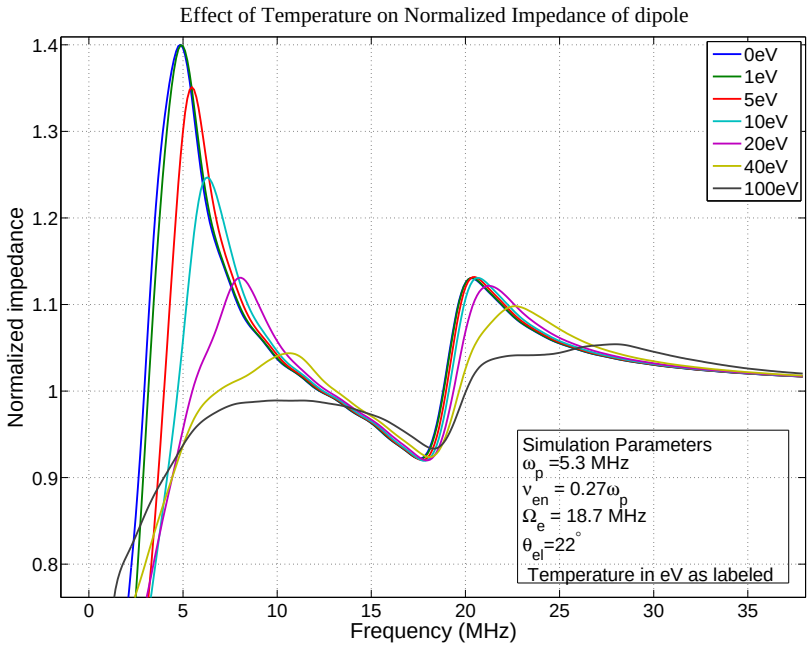

Fig. 5.6: Impedance of a dipole antenna in a homogeneous plasma for different values of electron temperature as simulated by PF-FDTD.

made of 26 cells of cell size dx=0.04) are shown in fig. 5.8. Separate plasma resonances which may correspond to the two regions can be seen instead of the single plasma frequency peak seen in the homogeneous case.

The aerodynamic structure around a fast moving rocket can be roughly approximated as a cone with gradually varying electron density in the wake region. The impedance of the 1.04 m dipole in a symmetric conical background density profile approximating the flow structure around a spacecraft was simulated and the result is shown in fig. 5.9. The symmetric density variation cone was within the simulation box for the test case as shown in fig. 5.10. This minor modification provides the PF-FDTD simulation with the capability to simulate a conical structure of any size and strength of density gradients. The impedance curve for the conical structure too like the discontinuity cases shows marked differences from the homogeneous case near the plasma resonance. These results confirms that the ambient density structure affects the impedance of PIP and needs to be accounted for during the analysis of any impedance data from instruments on-board sounding rockets.

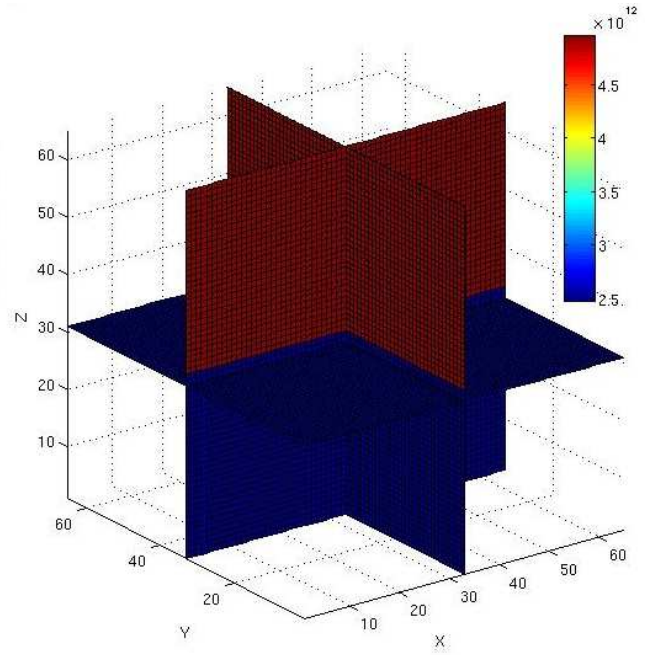

Fig. 5.7: Background electron density representing a boundary between two different plasma regions.

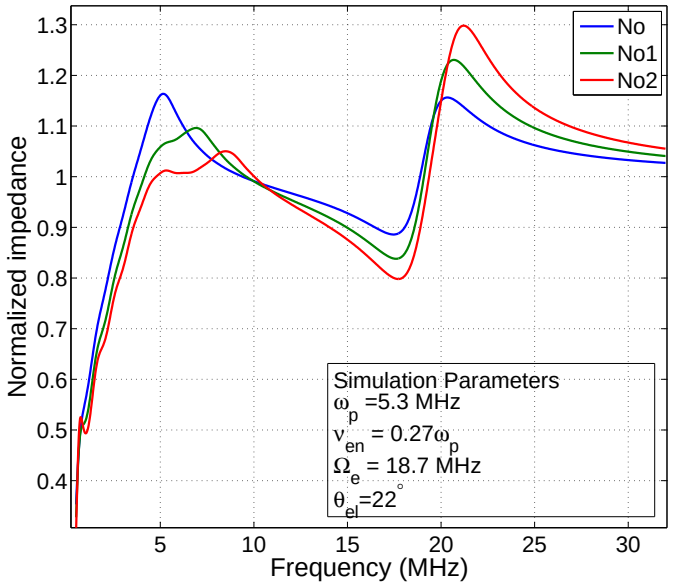

Fig. 5.8: Simulated impedance of a dipole antenna in a plasma with discontinuity at the middle of the dipole. The figure shows comparison between homogeneous case (No) and discontinuity cases of different strengths ($No1 = 2 \times No$ and $No2 = 3 \times No$).

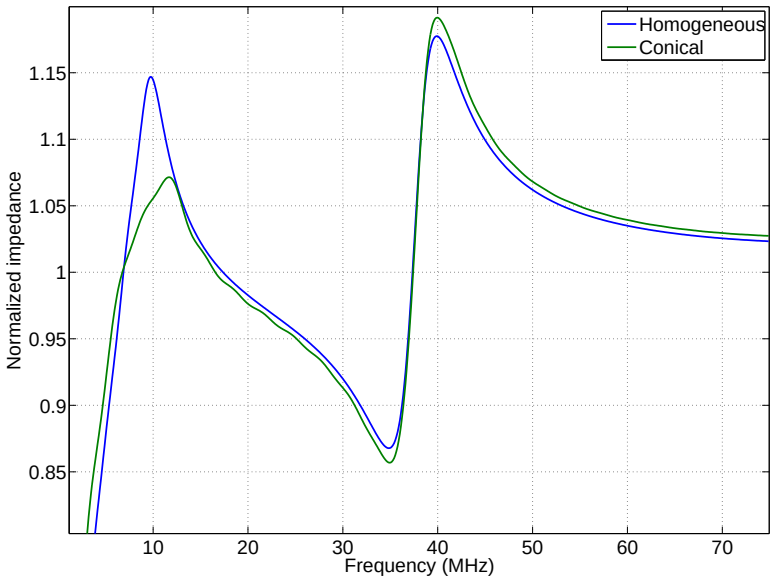

Fig. 5.9: Comparison of impedance of a dipole antenna in a homogeneous plasma and in plasma with an embedded conical density variation.

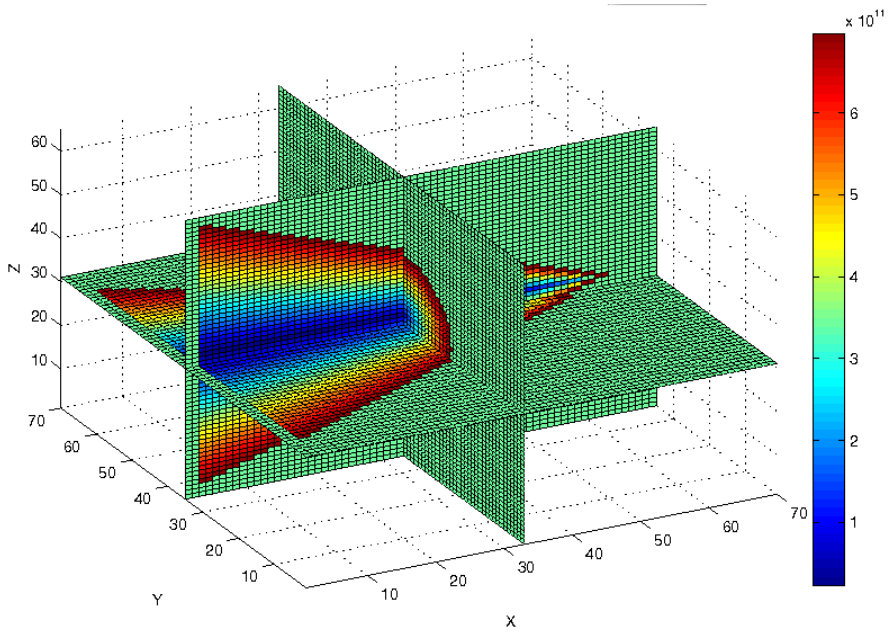

Fig. 5.10: Background electron density in the PF-FDTD simulation box of $70 \times 70 \times 65$ cells showing a conical electron density distribution that approximates the flow structure simulated by DSMC.

5.4 Aerodynamic Effects

The aerodynamic word comes from two Greek words: aerios, concerning the air, and dynamis, which means force. Aerodynamics effects caused by the supersonic motion of a sounding rocket affects atmospheric in-situ measurements.

5.4.1 Spin Modulation

Density measurements on spinning spacecrafts are contaminated by the spin modulation effects. The accrued errors introduced in the measurement is due to three separate processes. Satellite wake effect modulation at the spin rate, geomagnetic field effects at twice the spacecraft spin frequency and symmetric about the magnetic field vector which occur as a result of difference in plasma conductivity parallel and perpendicular to the geomagnetic field lines, and $\mathbf{v}\&\mathbf{B}$ effects at the spin frequency due to the induced potential difference between the sensor and the rocket axis. If the rocket attitude information throughout its trajectory is available, then the geomagnetic effects can be quantified by both Balmain's theory and PF-FDTD. But in many cases as in the SAL mission the attitude data is not available. The magnitude of the induced potential difference between the sensor and satellite axis depends on the orientations of the satellite spin axis, satellite velocity vector, and the geomagnetic field vector. Errors up to 20% have been reported due to this effect [42]. The most dominant of these effects is due to the satellite wake structure [42] and is the only effect considered for this study.

Spin modulation due to spacecraft wake structure in density measurements is observed whenever side looking instruments, either on rocket surface or on radially directed booms move in and out of the asymmetric density structure. As the rocket moves along its trajectory, if its nose is not aligned perfectly with the ram direction then an asymmetric wake is formed behind it. This wake structure is dependent on the angle with respect to the ram side, density, velocity, and the geometry of the spacecraft. The wake structure can be described by the ratio n_m/n_0 as a function of position in the wake where n_m and n_0 are the measured and unperturbed number density, respectively. But in most measurements the ambient unperturbed electron density value is not known a-priori, and hence the ex-

act wake structure can only be inferred by solving the inverse problem of matching the measured impedance to the simulated impedance in the predicted wake environment.

The DSMC simulation used for predicting the flow structure around SAL only reflects the effects due to neutral particles. There are numerical and theoretical models for predicting plasma wake, but most numerical models tend to be time-consuming, rendering them less useful for data analysis. At the present time there is no agreed-upon theoretical model which describes the temporal and spatial distribution of charged particles and fields around a spacecraft under realistic conditions, particularly not for the wake region. Hence, assuming strong collisional coupling between the charged particles and the neutrals at mesospheric altitudes, the individual species wake structure would be strongly affected by the neutral wake. We approximate the electron wake structure formed around a spacecraft by assuming a structure similar to the neutral wake structure on the downleg of SAL rocket at 92.5 km as predicted by the DSMC simulation of Aroh [17]. The SAL rocket was at an angle of 2° and 8° on the downleg with respect to the ram-side at 92.5 km. The approximate asymmetric conical density is shown in figs. 5.11 and 5.12, the orthogonal slice planes show the 3-D distribution of density in the simulation box.

In order to reproduce the spin modulation effect similar to that observed on SAL data using the PF-FDTD simulation, we rotate the asymmetric conical background density structure of fig. 5.11 by 360 degrees in steps of 45 degrees. These steps mimic the motion of the radial dipole on the rotating rocket with a constant asymmetric wake around it. The bottom view of the rotating conical structure and the corresponding angle of rotation are shown in fig. 5.13. The resulting impedance curves are shown in fig. 5.14.

Balmain's analytical theory [10] is used to compare the simulated impedance curves following the technique explained by Spencer et al. [2]. The ambient density value for the simulations was chosen close to the values observed during the upleg of the SAL mission at 97 km as shown in fig. 5.2. For the standard least mean square matching procedure with balmain using an evolutionary algorithm, two matching criterion were used:

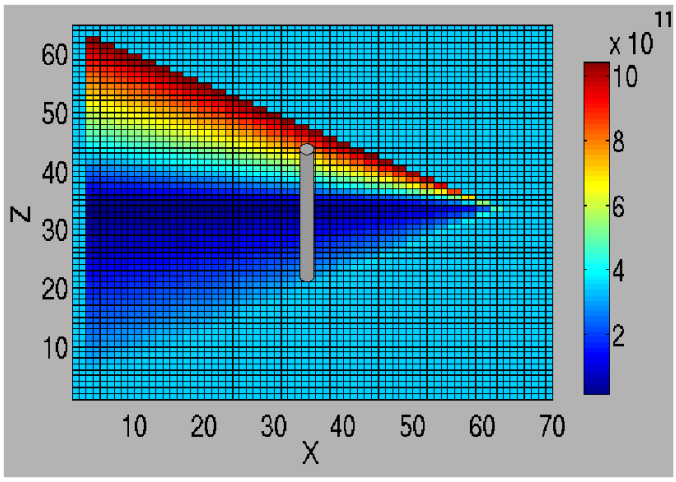

Fig. 5.11: Background electron density in the PF-FDTD code showing the side sectional view of the conical density variation. A dipole has been superimposed to illustrate the location of the dipole inside the simulation box.

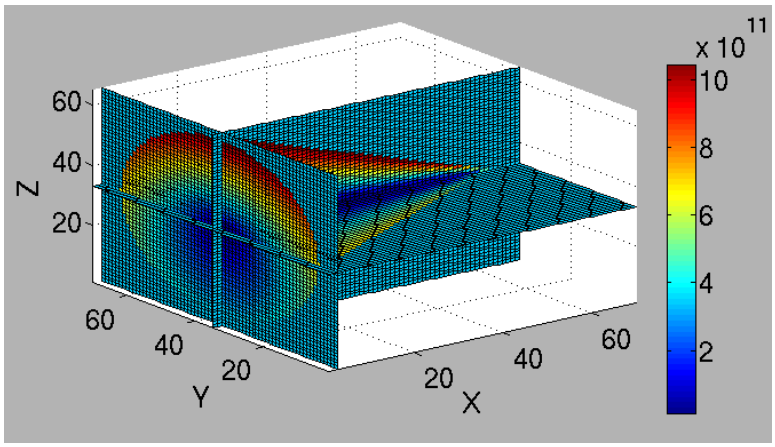

Fig. 5.12: Background electron density in the PF-FDTD code showing a conical density variation approximating the flow structure simulated by DSMC for SAL at 92.5 Km downleg 8° to ram.

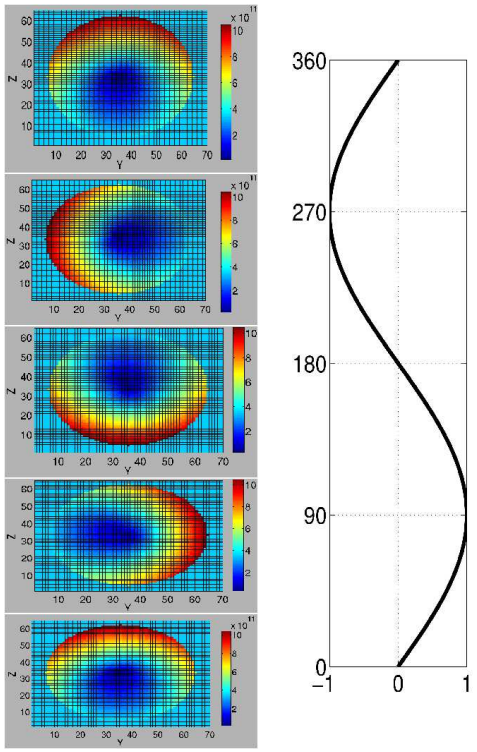

Fig. 5.13: Graphic showing one complete rotation of the asymmetric inhomogeneous conical structure.

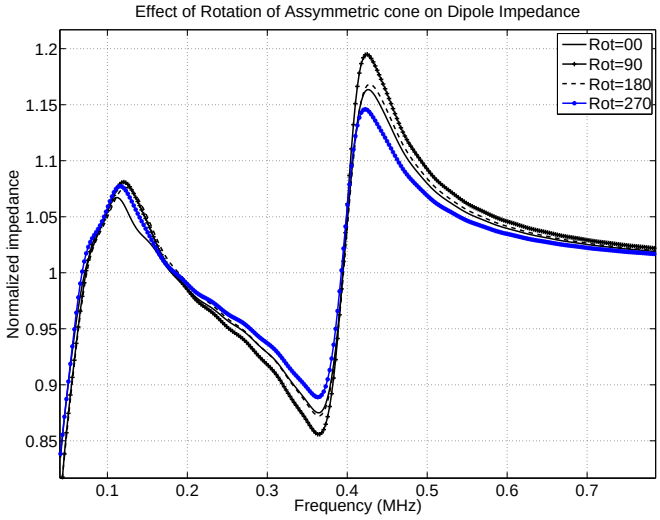

Fig. 5.14: Impedance of a dipole antenna as predicted by PF-FDTD in an asymmetric cone as the cone is rotated to simulate rocket spin.

a) Balmain's theory is used for matching over the entire range of frequencies encompassing the plasma resonance to the upper hybrid resonance, and higher.

b) Matching only for frequencies higher than the upper hybrid frequency (ω_{uh}).

A clear sine dependence with the angle of rotation, of the amplitude of the normalized simulated impedance curve is seen for the regions of the curves higher than Ω_{ce} frequency as shown in fig. 5.14. No such dependence is seen near the plasma resonance. The two matching conditions are employed to estimate the effect of this behavior on the impedance data analysis. The extracted plasma frequency values are close to the spin modulated values observed during the SAL mission at an altitude of 97 km. There is a small difference in the results obtained under the two matching conditions as seen in panel (a) fig. 5.15, also shown in panel (b) fig. 5.15 is a zoomed section of SAL spin modulation at 97 km on the upleg for comparison. Results from the matching of the entire curve show asymmetry in the density values about the ambient density assumed, but both the results clearly predict the spin modulation in the density values. This result shows an example of uncertainty in the data analysis. Running average smoothing of the spin modulation observed with the first matching condition will give values different from the assumed ambient density value.

5.4.2 Correction of the Aerodynamic Effects

A relevant flow simulation like DSMC or a PIC simulation should be used to accurately predict the flow structure around the rocket depending on the regime of operation. The derived density values then can be exported to PF-FDTD to calculate the impedance. Relative density variations can be calculated as explained in the previous section. The spin modulations from the observations and the PF-FDTD simulations at the altitude under observations should then be compared. The correction is done by dividing the measured density by the relative density from the simulation. The results are then smoothed of noise by a running average, which in this case will not lead to any significant loss of information.

5.5 Conclusions and Future Work

In this paper, a technique to derive absolute electron densities from impedance probe

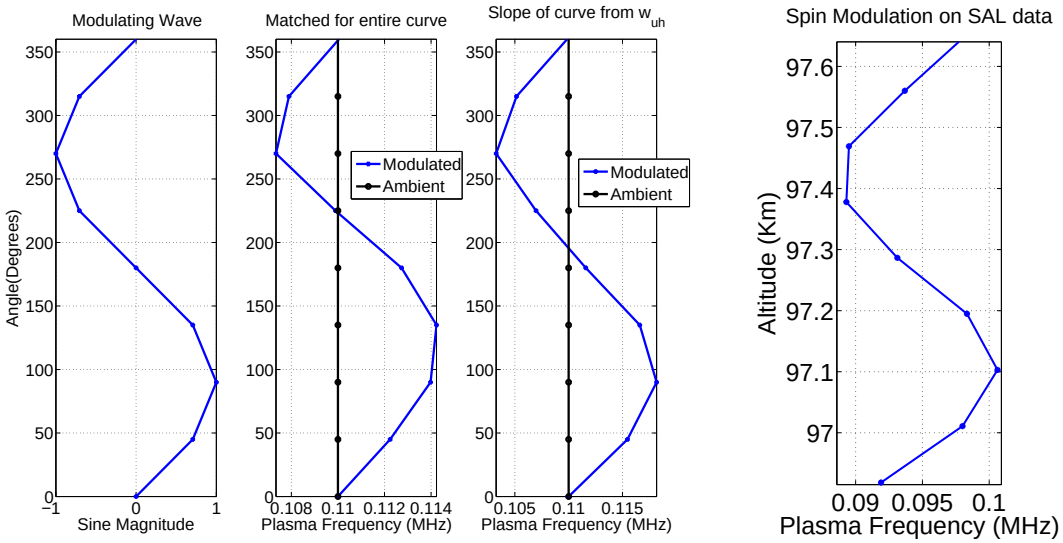

(a) **(b)**

Fig. 5.15: Left panel (a) shows derived plasma frequencies from the impedance curves for different values of cone rotation. The first figure on the left shows the modulating wave. Figure in the center shows the result of matching for the entire curve while the last figure shows the results for matching only frequencies higher than the upper hybrid frequency. Right panel (b) shows spin modulation observed on the upleg of SAL data.

data on sounding rockets was presented. Knowing the flow conditions during an entire flight and simulating the wake structures should help us in removing the spin modulation from density measurements.

The PF-FDTD code can now not only be used to analyze impedance data from sounding rockets and orbiting satellites, but also be used to verify analytical models of charged spacecraft wake. Presence of a second harmonic in the amplitude spectrum of the derived density with spin modulation in fig. 5.3, seems to suggest that more than one phenomenon might have contributed to the errors in density meaurements. Future studies can be done to analyze the effects of geomagnetic fields which occur at twice the rocket spin rate, to find any correlation with the second harmonic observation.

Chapter 6

Summary and Conclusions

6.1 Summary

Interaction of an antenna in a plasma environment and quantifying its effects on the antenna impedance has been used as a plasma diagnostic tool for many decades. While the measurement technique is fairly well developed, the interpretation of the impedance data poses challenging problems. The measured data is normally compared to analytical formulas for the impedance obtained through mathematical techniques. The major weakness of the analytical theories are that they do not self-consistently calculate the current distribution along the dipole. The PF-FDTD code computes the current distribution on the antenna structure self-consistently, thus providing a more accurate model for analysis of the measured impedance.

In Chapter 3, using Balmain's analytical theory as rough guide, the PF-FDTD simulation is used to analyze impedance data from the SAL sounding rocket mission. The measured impedance curve is most reliable above the cyclotron frequency Ω_{ce}. However, the data has some oscillation, through our selection of upper, median, and lower envelopes, we provide error bounds for values of the plasma parameters. The electron neutral collision frequency is obtained from the analysis and the results are up to 20% more accurate than the values predicted by Balmain. Chapter 4 explains the frequency scaling property of the linearized PF-FDTD code and how that can be used as a useful means of reducing computation time. An algorithm to automate the data reduction technique used for the analysis of Chapter 3 is also explained.

The second paper presented in Chapter 5 presents a qualitative analysis of the aerodynamic effects on the dipole antenna impedance. The PF-FDTD simulation is modified to incorporate the effects of inhomogeneous plasma. The asymmetric flow over a sound-

ing rocket is approximated as asymmetric conical background electron density by assuming strong collisional coupling between neutral and charged particles at mesospheric altitudes. A qualitative study of the spin modulation due to spacecraft aerodynamics observed on SAL sounding rocket PIP data is performed using an asymmetric conical density structure in the PF-FDTD simulation. A methodology for correction of aerodynamic effects is explained which should be useful for demodulating any spin modulations observed on future sounding rocket missions.

6.2 Future Work

The capability of PF-FDTD simulation to model any antenna impedance in inhomogeneous plasma provides researchers with a valuable tool to validate analytical theories and analyze experimental results. Results of analytical and numerical charged wake structure models can be incorporated in the simulation to improve the present understanding of antennas in plasma. Effects of shock fronts and shape of the wake structure on antennas can be modeled. Although the model opens up many areas of prospective research, the performance of PF-FDTD must be evaluated for effects changing density on the boundary conditions. To be effective as a tool for monitoring of the plasma during dry etch process or any high density plasmas, it needs to be validated at high frequencies where the antenna starts radiating.

The main deterrent to using PF-FDTD for large sets of impedance data is the computation time required. Simulation time limits the usage of PF-FDTD to analyzing relatively small data sets. Reduction in the simulation time can be achieved by efficient utilization of memory allocation and parallelzing the finite difference calculations. This will allow the simulation to be used for analyzing the impedance over the entire flight path.

Analytical theories can be improved by comparing their outputs to that of PF-FFDTD simulations. Proper modeling of the current distribution along the antenna surface using the self-consistent PF-FDTD model may provide vital information in revealing the cause of discrepancies between experimental data and theories.

References

[1] J. Ward, *The Numerical Modelling of an Antenna in Plasma*. Ph.D. dissertation, Utah State University, Logan, UT, 2006.

[2] E. Spencer, S. Patra, T. Andriyas, C. Swenson, J. Ward, and A. Barjatya, "Electron density and electron neutral collision frequency in the ionosphere using plasma impedance probe measurements," *Journal of Geophysical Research*, vol. 113, no. A09305, Sept. 2008.

[3] C. A. Balanis, *Antenna Theory Analysis and Design*, 2nd ed. New York: John Wiley and Sons, 1997.

[4] R. F. Pfaff, *Modern Ionospheric Science*, ch. 16. Katlenburg-Lindau, Germany: Copernicus Publication, 1996.

[5] W. Pfister, "Survey of RF impedance probes," ser. Direct Aeronic Measurements in Lower Ionosphere, vol. Aeronomy Report 1. Urbana, IL: University of Illinois, Dec. 1963.

[6] K. D. Baker, A. M. Despain, and J. C. Ulwick, "Simultaneous comparison of rf probe techniques for determination of ionospheric electron density," *Journal of Geophysical Research*, vol. 71, no. 3, pp. 935–944, 1966.

[7] R. H. Bishop and K. D. Baker, "Electron temperature and density determination from RF Impedance probe measurements in the lower ionosphere," *Planetary and Space Science*, vol. 20, pp. 997–1013, 1972.

[8] J. Galejs, "Impedance of a finite insulated cylindrical antenna in a cold plasma with a longitudinal magnetic field," *IEEE Transactions on Antennas and Propagation*, vol. AP-14, no. 6, pp. 737–748, Nov. 1966.

[9] H. Staras, "The Impedance of an electric dipole in a magneto-ionic medium," *IEEE Transactions on Antennas and Propagation*, vol. AP-12, no. 6, pp. 695–702, Nov. 1964.

[10] K. G. Balmain, "The impedance of a short dipole antenna in a magnetoplasma," *IEEE Transactions on Antennas and Propagation*, vol. 12, no. 5, pp. 605–617, Sept. 1964.

[11] K. G. Balmain, "Dipole admittance for magnetoplasma diagnostics," *IEEE Transactions on Antennas and Propagation*, vol. 17, no. 3, pp. 389–392, May 1969.

[12] J. Ward, C. M. Swenson, and C. Furse, "The impedance of a short dipole antenna in a magnetized plasma via a finite difference time domain model," *IEEE Transactions on Antennas and Propagation*, vol. 53, no. 8, pp. 2711–2718, Aug. 2005.

[13] K. S. Yee, "Numerical solution of inital boundary value problems involving maxwell's equations in isotropic media," *IEEE Transactions on Antennas and Propagation*, vol. 14, no. 3, pp. 302–307, 1966.

[14] A. Taflove and S. Hagness, *Computational Electrodynamics: The Finite-Difference Time-Domain Method*. Norwood, MA: Artech House, 2005.

[15] R. Heelis, "Electrodynamics in the low and middle latitude ionosphere: a tutorial," *Journal of Atmospheric and Solar Terrestrial Physics*, vol. 66, pp. 825–838, 2004.

[16] B. Oliver, R. Clements, and P. Smy, "Experimental investigation of the low-frequency capacitive response of a plasma sheath," *Journal of Applied Physics*, vol. 44, pp. 4511–4517, 1973.

[17] A. Barjatya and C. Swenson, "Observation of triboelectric charging effects on Langmuir-type probes in dusty plasma," *Journal of Geophysical Research*, no. A10302, Oct. 2006.

[18] D. D. Blackwell, D. N. Walker, S. J. Messer, and W. E. Amatucci, "Characteristics of the plasma impedance probe with constant bias," *Physics of Plasmas*, vol. 12, no. 093510, Sept. 2005.

[19] D. D. Blackwell, D. N. Walker, and W. E. Amatucci, "Measurement of absolute electron density with a plasma impedance probe," *Review of Scientific Instruments*, vol. 76, no. 023503, Jan. 2005.

[20] D. D. Blackwell, D. N. Walker, S. J. Messer, and W. E. Amatucci, "Antenna impedance measurements in a magnetized plasma II Dipole antenna," *Physics of Plasmas*, vol. 14, no. 092106, Sept. 2007.

[21] C. G. Carlson, "Next generation plasma frequency probe instrumentation technique," Master's thesis, Utah State University, Logan, UT, 2004.

[22] C. G. Carlson, C. M. Swenson, and C. Fish, "Next generation plasma impedance probe instrumentation technique," *American Geophysical Union Fall Meeting Abstracts*, p. B1106, 2003.

[23] D. E. Rowland, R. F. Pfaff, P. Uribe, and J. Burchill, "Plasma Impedance Spectrum Analyzer (PISA): an advanced impedance probe for measuring plasma density and other parameters," *American Geophysical Union Fall Meeting Abstracts*, p. A7, 2006.

[24] K. Sawaya, T. Ishizone, and Y. Mushiake, "Measurement of the impedance of a linear antenna in a magnetoplasma," *Radio Science*, vol. 13, pp. 21–29, Jan. 1978.

[25] B. Bhat and B. R. Rao, "Experimental investigation on the impedance behavior of a short, cylindrical antenna in a lossy magnetoplasma," *NASA Technical Reports Server*, vol. NASA-CR-107453,SR-2, 1969.

[26] P. Nikitin and C. Swenson, "Impedance of a short dipole antenna in a cold plasma," *IEEE Transactions on Antennas and Propagation*, vol. 49, no. 10, pp. 1377–1381, Oct. 2001.

[27] L. J. Gelinas, *An In-Situ Measurement of Charged Mesospheric Dust During a Sporadic a Sporadic Atom Layer Event*. Ph.D. dissertation, University of New Hampshire, Durham, NH, 1999.

[28] R. W. Schunk and A. F. Nagy, *Ionospheres, Physics, Plasma Physics, and Chemisty*. New York: Cambridge University Press, 2000.

[29] S. W. H. Cowley, *Tutorial: Magnetosphere-Ionosphere Interactions: A Tutorial Review*, p. 91. Magnetospheric Current Systems, 2000.

[30] S. Chapman and T. G. Cowling, *The mathematical theory of nonuniform gases*. New York: Cambridge University Press, 1970.

[31] J. L. Chau and E. Kudeki, "First e- and d-region incoherent scatter spectra observed over jicamarca," *Annales Geophysicae*, vol. 24, pp. 1295–1303, July 2006.

[32] J. A. Bittencourt, *Fundamentals of Plasma Physics*. New York: Springer, 2004.

[33] N. Ivchenko, L. Facciolo, P. A. Lindqvist, P. Kekkonen, and B. Holback, "Disturbances of plasma environment in the vicinity of the astrid-2 microsatellite," *Annales Geophysicae*, vol. 19, pp. 655–666, 2001.

[34] P. Patterson, *In situ measurements of upper atmospheric atomic oxygen: The ATOX resonant fluorescence/ absorption sensor*. Ph.D. dissertation, Utah State University, Logan, UT, 2005.

[35] E. Engwall, A. Eriksson, and J. Forest, "Wake formation behind positively charged spacecraft in flowing tenuous plasmas," *Physics of Plasmas*, vol. 13, pp. 062 904–062 904–10, 2006.

[36] G. Bird, *Molecular Gas Dynamics and the Direct Simulation of Gas Flows*. Oxford: Oxford University Press, 1994.

[37] J. Kurihara, K. I. Oyama, N. Iwagami, and T. Takahashi, "Numerical simulation of 3-d flow around sounding rocket in the lower thermosphere," *Annales Geophysicae*, vol. 24, pp. 89–95, 2006.

[38] J. Gumbel, "Aerodynamic influences on atmospheric in-situ measurements from sounding rockets," *Journal of Geophysical Research*, vol. 106, no. A6, pp. 10,553–10,563, 2001.

[39] J. Hedin, J. Gumbel, and M. Rapp, " On the efficiency of rocket-borne particle detection in the mesosphere," *Atmospheric Chemistry and Physics*, vol. 7, no. 3701-3711, July 2007.

[40] G. Odmark, "Effects of suborbital space flights (ii). a study of spacecraft charging," Master's thesis, Royal Institute of Technology, Stockholm, 2007.

[41] A. Barjatya, *Langmuir Probe Measurements in the Ionosphere*. Ph.D. dissertation, Utah State University, Logan, UT, 2007.

[42] C. V. Goodall, H. D. Hopkins, Y. Kabasakal, and R. J. D'Arcy, "Topside ionosphere electron density measurements on ariel 4," *Proceedings of the Royal Society of London*, vol. 343, pp. 189–206, 1975.